PHYSICAL REVIEW B VOLUME 26, NUMBER 8 15 OCTOBER 1982

Determination of the elastic constants of single crystals of fcc and hcp argon alloys by Brillouin scattering

S. F. Ahmad, H. Kiefte, M. J. Clouter, and M. D. Whitmore
Department of Physics, Memorial University of Newfoundland, St. Johns, Newfoundland A1B 3X7 Canada
(Received 10 March 1982)

The elastic constants of single crystals of $Ar(O_2)$ and $Ar(N_2)$ alloys, both for the fcc and hcp structures near their melting points, have been accurately determined using high-resolution Brillouin spectroscopy. The elastic constants were found to be relatively insensitive to changes in the concentration of O_2 (and N_2) up to about 4% in the fcc phase. Mode softening was, however, reflected in the dependence of c_{44} on solute concentration, as phase instability increased. The hcp elastic constants of $Ar(O_2)$ at 6% concentration at 81.3 K were determined to be (in units of 10^9 N m^{-2}): $c_{11}=2.90\pm0.04$, $c_{12}=1.50\pm0.03$, $c_{13}=1.18\pm0.02$, $c_{33}=3.24\pm0.05$, and $c_{44}=0.656\pm0.011$. Even at this high concentration the elastic constants are relatively consistent with pure Ar values, except for c_{13} and c_{13}/c_{44}. From model calculations it was shown that the observed differences cannot be explained either in the presence or absence of spherical O_2 impurity molecules. The use of nonspherical impurity interactions indicated that the anisotropy of the O_2 (and N_2) molecule plays a strong role in the intermolecular forces, the anomalous change in c_{13} was, however, not reproduced. It is concluded, also on the basis of further experimental and theoretical evidence, that rotation-translation coupling is an important mechanism in van der Waals solids, especially for phase transitions, and that c_{13}/c_{44} (for hexagonal systems, at least) is a sensitive measure of this effect. This almost certainly defines the role of diatomic impurities in stabilizing the hcp Ar structure.

I. INTRODUCTION

The crystalline solid phases of the heavier rare gases (Ne, Ar, Kr, Xe) are among the simplest in nature. They have been the focus of extensive theoretical work because they can be represented by relatively simple models that are of importance in the development of the more general molecular theory of matter. For the most part, the agreement between theory and experiment for the rare gas solids is good, especially in the case of Ar.[1] There is an important exception,[2] however, in that existing theories consistently predict the hcp structure for these solids, whereas it has been well established experimentally that (excluding helium) the stable structure, is, in fact, fcc at all temperatures from the respective triple points to essentially 0 K. It is towards this point of interest that this work is directed.

Many attempts have been made to determine the possible deficiencies of the theoretical treatment that may be responsible for this discrepancy. It has been demonstrated that the use of two-body pair potentials with the inclusion of a three-body term, such as the Axilrod-Teller-Muto term, fails to predict the fcc structure.[3–9] Similar results were obtained from considerations of the zero-point energy (both harmonic and anharmonic[10–13]), the possibility of thermal transitions between the fcc and hcp structures in the quasiharmonic approximation,[14–16] and long-range many-body forces.[2,8,9] Although short-range many-body forces do give rise to the hcp structure in the investigations of Jansen and co-workers,[17] the use of Gaussian wave functions for the distribution of the atomic electrons in this case was found to be unrealistic.[18,2] Some qualitative suggestions have been made[6,19–21] that the angular dependence of the interatomic forces may account for the stability of the fcc structure. Niebel and Venables[22] also attempted to explain the stability of this phase by considering the possible effects of short-range overlap interactions. Their results received initial support from Bricheno and Venables,[23] who performed vapor-pressure measurements on fcc Ar and the hcp phases of $Ar(O_2)$ alloys in order to calculate the free-energy differences (Δ) between the two structures near the triple point. Subsequent research,[24] however, led to the conclusion that the variation of Δ with temperature could not be explained by this model alone, and it was suggested that a more detailed treatment of anharmonicity

(including the possibility of a nonideal c/a ratio) should be undertaken. Very recently it was pointed out by Borden and Radin[25] that one elementary aspect of the problem appears to have been overlooked; namely, the possible significance of different surface energies in finite samples of the two structures. Their calculations show that for a nearest-neighbor model, the surface energy per particle is lower for the fcc structure, and they conclude that this effect provides the needed explanation.

By comparison with the foregoing, relatively little attention has been paid to either the calculation or measurement of specific properties for the hcp phase, and this is most probably because the phase is difficult to produce in stable form. In fact, the only successful method was first employed by Meyer, Barrett, and co-workers,[26–31] who demonstrated that the doping of pure Ar with low concentrations of diatomics such as O_2, N_2, and CO can result in a stable hcp structure, Their application of powder diffractometry techniques resulted in detailed phase diagrams for these solid solutions, and the lattice constants were also determined as a function of solute concentration. In addition to the vapor-pressure measurements[23] already mentioned, Hägele *et al.*[32] measured birefringence in the hcp phase of $Ar_{0.98}(O_2)_{0.02}$, while Schuberth[33] observed first-order Raman scattering from such a hcp phase. Of particular relevance, however, is the fact that no investigation of the elastic properties of the above alloys (either hcp or fcc) has been reported.

Extensive theoretical research has been done on the heavier rare-gas solids in the undoped fcc phase, but very little attention has been paid to the hcp phase. During attempts to explain the stability of the fcc phase, some workers have calculated the differences in the specific heats and the Debye temperatures of the two phases, and the elastic constants of the hcp structure of pure Ar have been calculated[34] by the self-consistent harmonic approximation using Aziz's potential.[35] The latter are of importance in the present context since comparison of theoretically calculated elastic constants with the experimentally measured ones provides a very sensitive test of any potential predicted for the substance and for the lattice-dynamical theory used to predict the solid properties.

Given the clear lack of relevant data, it was decided to undertake a series of accurate measurements of the elastic constants for doped fcc and hcp crystals of Ar. It was hoped that by extrapolating the results to the case of pure Ar, some clarification of the role of the impurity in stabilizing the hcp structure would be forthcoming, and that this in turn would lead to a better understanding of the interactions involved in the two (impurity-free) structures. The Brillouin scattering technique offers special advantages in the case of these difficult-to-produce samples, since only small single crystals are required, and highly accurate values of the (adiabatic) elastic constants can be obtained without disturbing the crystal in any mechanical sense.

Single crystals of Ar doped with O_2 and N_2 were grown both in the fcc and the hcp phases,[36] and the subsequent procedures were, in brief, as follows. First, the quality of each crystal, as well as its phase and orientation with respect to the laboratory frame of reference, were determined by the Laue x-ray transmission method. Brillouin spectra were then recorded at temperatures just below the freezing point in each case, and a series of different orientations was employed so that the Brillouin shifts (and hence the sound velocities) could be measured for various directions in each crystal. The elastic constants were then determined in accordance with the discussion below.

A. Resumé of Brillouin scattering in single crystals

The theory of Brillouin scattering has been discussed by many authors.[37] The scattering of light can be attributed to those inhomogeneities, or fluctuations, in the optical dielectric constant of the scattering medium that are associated with the propagation of thermally excited sound waves. Using such classical arguments, Benedek and Fritsch[38] presented a theory of Brillouin scattering in crystals of cubic symmetry, and the same has been extended to include hexagonal crystals by Hamaguchi.[39] Nelson *et al.*[40] presented a general theory of Brillouin scattering that is valid for anisotropic crystals of any symmetry. These theories successfully predict the intensity, polarization, and frequency shift of the scattered light with the result that (for a crystal) the spectrum consists of three sets of doublets located symmetrically about the incident frequency. The frequency shifts are given by[38]

$$\nu_\mu = \pm 2\frac{n}{c}\nu_0 V_\mu(\vec{q})\sin\left[\frac{\theta}{2}\right], \tag{1}$$

where ν_0 is the frequency of the incident radiation, ν_μ and V_μ are the frequency and phase velocity,

respectively, for the μth acoustic mode of wave vector $\vec{q}$, n is the index of refraction of the medium, c is the velocity of light in vacuum, and θ is the (measured) scattering angle. With the assumption in particular, that the value of n is known, this equation can be used to obtain the values of V_μ from the frequency shifts in the observed spectra. It should be noted that, for ν_0 values in the visible region and $\theta \simeq 90°$, the ν_μ are typically in the *hypersonic* (GHz) range, so that it is the *adiabatic* elastic constants that are eventually determined from the data.

When the equation of motion for elastic wave propagation in a crystal is solved, the result obtained is[41]

$$(\rho\omega^2\delta_{il} - c_{ijkl}q_j q_k)\hat{\Pi}_l = 0 , \tag{2}$$

where ρ is the density, ω is the angular frequency, δ_{il} is the Kronecker delta, c_{ijkl} represents the elastic constant tensor, and $\hat{\Pi}$ is the polarization vector of the sound wave. This is a cubic equation in ω^2 and yields three eigenvalues (corresponding to $\mu = 1,2,3$) from which the sound velocities are obtained as

$$\vec{V}_\mu(\vec{q}) = \omega_\mu(\vec{q})\hat{q}/|\vec{q}| . \tag{3}$$

The three acoustic modes are identified according to their predominant polarization characteristics as the "slow" transverse mode T_1, the "fast" transverse mode T_2, and the longitudinal mode L.

For hexagonal crystals the elastic constant tensor reduces to five independent constants, designated c_{11}, c_{12}, c_{13}, c_{33}, and c_{44}, so that (2) can be written in the closed form[41]

$$\begin{aligned}
\rho V^2(T_1) &= \tfrac{1}{2}(c_{11}-c_{12})\sin^2\gamma + c_{44}\cos^2\gamma , \\
\rho V^2(T_2) &= \tfrac{1}{2}(c_{11}\sin^2\gamma + c_{33}\cos^2\gamma + c_{44} - \Phi) , \\
\rho V^2(L) &= \tfrac{1}{2}(c_{11}\sin^2\gamma + c_{33}\cos^2\gamma + c_{44} + \Phi) , \\
\Phi^2 &= [(c_{11}-c_{44})\sin^2\gamma + (c_{44}-c_{33})\cos^2\gamma]^2 \\
&\quad + 4(c_{13}+c_{44})^2\sin^2\gamma\cos^2\gamma ,
\end{aligned} \tag{4}$$

where γ is the angle between the c axis of the crystal and the acoustic wave vector $\vec{q}$. In this work the elastic constants of hcp crystals were determined by using a least-squares-fitting procedure to effectively invert Eqs. (4). Although for fcc crystals the number of independent elastic constants reduces to three (i.e., c_{11},c_{12},c_{44}), the general closed-form relations are not as simple as (4).[42] Consequently, the elastic constants were obtained in these cases by applying orthogonal matrix transformation methods to solve Eq. (2).

It is of interest to note that in general, these crystals are elastically anisotropic, so that all three modes are nondegenerate for an arbitrary choice of propagation direction. In the fcc case the extent of this anistropy is indicated by the parameter

$$A = 2c_{44}/(c_{11}-c_{12}) , \tag{5}$$

where $A = 1$ for the isotropic crystal. In the case of an isotropic hcp crystal the following additional relations hold[43]:

$$\begin{aligned}
c_{44} &= \tfrac{1}{2}(c_{11}-c_{22}) , \\
c_{11} &= c_{33} , \\
c_{11}+c_{12} &= c_{13}+c_{33} .
\end{aligned} \tag{6}$$

B. Relationships between fcc and hcp elastic constants

Given the objectives that have already been stated with respect to the phases of pure Ar, two further problems were encountered. First, since it was found that the hcp phases of Ar(O_2) and Ar(N_2) could not be produced with solute concentrations less than 5 and $4\frac{1}{2}$ mol %, respectively,[36] the extrapolation of the (hcp) elastic constant data to zero solute concentration could not be performed experimentally. Rather, it was necessary to address this problem on theoretical grounds by attempting to calculate the effect of the impurities on the elastic constants (see Sec. V). Second, and not withstanding the extrapolation problem, it was necessary to determine a meaningful way of comparing the two fundamentally different sets of fcc and hcp elastic constants.

Fortunately, this (latter) problem has been encountered in a somewhat broader context, and has been the subject of a number of publications.[44–48] Novotny and Smith[45] compared the elastic constants of the fcc and hcp allotropes of thallium by employing a trigonal representation for both structures. The hexagonal elastic constants were related to the constants in the trigonal representation with the symmetry constraint that c_{14} be zero. The same procedure was followed by Leamy and Warlimont[46] in comparing the elastic constants of fcc and hcp cobalt. A further step was taken by Martin,[47] who derived a transformation which related the second-order elastic constants of tetrahedrally coordinated compounds, cubic zinc blende (ZnS), and hexagonal wurtzite (ZnS). Fuller and Wes-

ton[48] then extended this theory to the third-order elastic constants for the same two structures of CdS. They also applied the transformations to the fcc and hcp elastic constants of polymorphic metals and found good agreement with the experimental results.

In this paper the transformations as given by Martin[47] are used to compare the elastic constants of the hcp and fcc phases of Ar. The latter structures can both be constructed from suitably defined tetrahedral building blocks. The fcc structure is formed by aligning these tetrahedra in equivalent directions, whereas in the hcp structure, they are alternately aligned in two inequivalent orientations which are rotated 180° with respect to each other.[49] As a first step in the transformation, the fcc elastic tensor is rotated to each of the two trigonal orientations composing the hcp structure. The coordinate axes X, Y, and Z for the fcc crystal were taken to be in the $\langle 100\rangle$, $\langle 010\rangle$, and $\langle 001\rangle$ directions, and for the triagonal representation in the $\langle 110\rangle$, $\langle 112\rangle$, and $\langle 111\rangle$ directions. The average trigonal elastic constants $\bar{c}_{ij}$ in terms of fcc values c_{ij}^F are given by (see Refs. 47 and 48)

$$\begin{aligned}
\bar{c}_{11} &= (c_{11}^F + c_{12}^F + 2c_{44}^F)/2 , \\
\bar{c}_{12} &= (c_{11}^F + 5c_{12}^F - 2c_{44}^F)/6 , \\
\bar{c}_{33} &= (c_{11}^F + 2c_{12}^F + 4c_{44}^F)/3 , \\
\bar{c}_{13} &= (c_{11}^F + 2c_{12}^F - 2c_{44}^F)/3 , \\
\bar{c}_{44} &= (c_{11}^F - c_{12}^F + c_{44}^F)/3 , \\
\Delta_{14} \equiv \bar{c}_{14} &= (c_{11}^F - c_{12}^F - 2c_{44}^F)/3\sqrt{2} .
\end{aligned} \tag{7}$$

The conversion from cubic to hexagonal elastic constants c_{ij}^H is then completed by using two internal strain corrections I_1 and I_2 as follows:

$$\begin{aligned}
c_{11}^H &= \bar{c}_{11} - I_1 , \quad c_{13}^H = \bar{c}_{13} , \\
c_{12}^H &= \bar{c}_{12} + I_1 , \quad c_{33}^H = \bar{c}_{33} , \\
c_{44}^H &= \bar{c}_{44} - I_2 ,
\end{aligned} \tag{8}$$

where

$$\begin{aligned}
I_1 &= \Delta_{14}^2/\bar{c}_{44} , \\
I_2 &= \Delta_{14}^2/[\tfrac{1}{2}(\bar{c}_{11} - \bar{c}_{12})] .
\end{aligned}$$

It is important to note that c_{13}^H and c_{33}^H are independent of internal strains. The above relations form the basis for the discussion of experimental results in Sec. IV C.

II. EXPERIMENTAL METHOD

A. Cryostat and the sample cell

Figure 1 shows a schematic diagram of the apparatus used in these experiments. The crystals were grown in a vacuum-insulated cell contained within a modified commercial liquid-He cryostat (Janis Research Co., Model 10DT). Figure 2 shows the top and tail sections of the cryostat. The sample cell was soldered to a 1-m-long stainless steel tube, which was suspended and centered in the inner bore of the cryostat. At the top it was connected to an appropriate gas handling, mixing, and filtering system. The topmost portion of the cryostat allowed for easy, accurately measurable, rotation of the sample cell, and the crysotat tail section was readily removable for access to the cell region.

Liquid helium from the main reservoir was admitted through a capillary tube to a heat exchanger, in close proximity to the cell, and the flow could be adjusted by a needle valve. The sample cell was attached to the heat exchanger via flexible copper braids. For additional temperature control, a resistance heater wire of 50 Ω was wound around the heat exchanger, the temperature at this point being measured by a screw-mounted GaAs temperature sensor.

The sample cell was surrounded by two polished aluminum radiation shields, The inner shield was maintained at the same temperature as the heat exchanger (usually 4 to 5 K below the cell tempera-

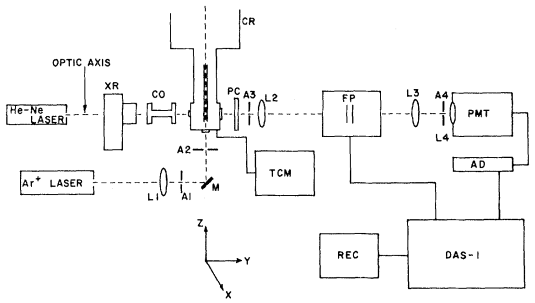

FIG. 1. Block diagram of the experimental arrangement for Brillouin scattering and x-ray diffraction, XR x-ray source, CO collimator, CR cryostat, PC polaroid land camera, $A1-A4$ apertures, $L1-L4$ lenses, M mirror, FP triple-pass Fabry-Perot interferometer, PMT cooled photomultiplier tube, AD amplifier-discriminator, DAS-1 data acquisition and stabilization system, REC strip chart recorder, TCM temperature control and measurement, He-Ne laser defines optic axis, and Ar^+ laser single-mode source of incident radiation.

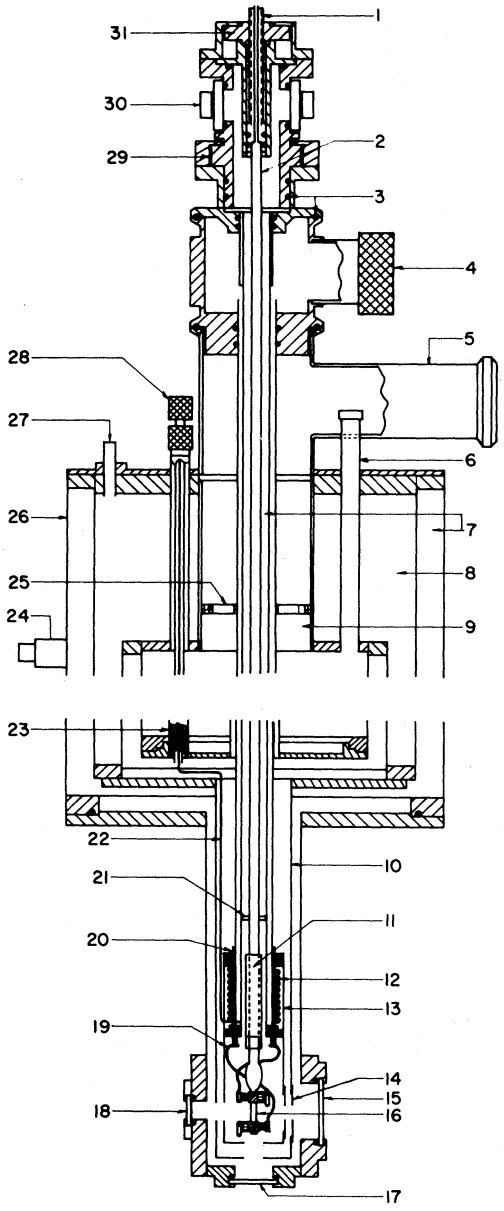

FIG. 2. Diagram showing cryostat and cell, 1 inlet tube, 2 stainless steel tube, 3 O-rings, 4 He recovery from heat exchanger, 5 He recovery from reservoir, 6 liquid-He fill, 7 vacuum, 8 liquid-N_2 reservoir, 9 liquid-He reservoir, 10 and 13 radiation shields, 11 dust collector assembly, 12 heater wires, 14 aluminum foil, 15 Plexiglass large window, 16 quartz sample cell, 17 quartz window, 18 Plexiglass small window, 19 copper braids, 20 heat exchanger, 21 Teflon spacer, 22 liquid-He capillary, 23 needle valve, 24 electrical feedthrough, 25 thermal anchor, 26 stainless steel outer wall, 27 liquid-N_2 fill and vents, 28 needle valve control, 29 rotary seal for rotating sample cell, 30 electrical feedthrough, and 31 raising and lowering assembly.

ture). The outer shield was maintained at liquid-nitrogen temperature. Flat-black paint was strategically applied to reduce stray light scattering.

The vertically incident laser beam entered the cryostat through a polished quartz window at the bottom of the cryostat. The light scattered from the cell, at 90° to the laser beam, was collected through a large side window made of Plexiglass for optimum transmission of x-radiation (as well as visible light) and provided a diffraction cone of $\sim 45°$ for photographic recording of transmission Laue patterns.

The sample cell itself consisted of a cylindrical quartz tube of 3 mm i.d. and 5 mm o.d. The tube was 2 cm in length and was fitted with a quartz-to-Kovar graded seal at the top. Because of problems with dust particles settling on the bottom window, a "dust trap" was installed between the sample cell and the inlet tube. (A brief description and a schematic diagram of the cell is given in Ref. 36.) The lower end of the cell was sealed with a highly polished quartz plug, 7 mm in length, utilizing epoxy resin cement (Lepages). This window performed two functions: (1) to let the incident laser light pass into the cell with minimum spurious scattering, and (2) to provide a cold spot as a nucleation site for formation of the crystal.

One copper braid was fastened with a phosphor-bronze spring clamp to the lower end of the cell, and a miniature GaAs diode was mounted on this clamp close to the quartz tube. The second braid was fastened with a similar spring clamp 1 cm above the lower one and a differential copper-constantan thermocouple was mounted across them. Resistance wires of 50 Ω were wound on each clamp to permit control of the cell temperature. All electrical wires and copper braids were so arranged that the x-rays as well as the light scattered along the axis of the collection optics was not blocked when the cell was rotated through about 120°.

Control of the cell temperature was effected in three stages: (1) by manually adjusting the flow of liquid He into the heat exchanger, (2) by electronically controlling the temperature of the heat exchanger, and (3) by electronically controlling the temperature of the spring clamps on the cell. For (2) and (3), proportional feedback controllers (Lakeshore Cryotronics, Inc., Model DTC500) were used in conjunction with the heaters and GaAs diodes mentioned above. In the stage (3) control, the main heater current was distributed between the top and the bottom heater on the cell by a simple potential divider. In this way a temperature

difference between the top and bottom clamps of the cell was maintained, thus providing the adjustable thermal gradient necessary for the growth of single crystals. The gradient was constantly monitored by the differential copper-Constantan thermocouple with a microvoltmeter (Keithley Instruments, Model 150B). The GaAs diode used to measure and control the cell temperature was calibrated *in situ* against the triple points of pure Ar, O_2, and N_2. The absolute calibration was estimated to be accurate within 0.2 K. The temperature of the cell was controlled to within ± 0.01 K over long periods of time, with a limitation being imposed by unavoidable fluctuations which accompanied the filling of the liquid-He reservoir at 50-h intervals.

B. Crystal growth, phase determination, and orientation

The gases used in the experiments were of research-grade quality and were supplied by Matheson Co. The nominal purity of the gases was, 99.99% for O_2 and 99.9995% for Ar and N_2. Edwards Model CG3 Speedivac pressure gauges were used to monitor the pressure in the cell, as well as to prepare the mixtures. Two 0.22-μm Millipore filters were also placed in the gas-handling system to help minimize dust problems. The percentages of O_2 and N_2 in Ar were determined at room temperature by taking the ratios of the partial pressures of each gas component to the total pressure of the gas mixtures. Mixtures were allowed to stand for about 48 h. The cell was then cooled slowly to 85 K in about 8—10 h when clear liquid filled the cell completely.

A modified Bridgeman method was used to grow single crystals. Details of the crystal growing technique and the associated problems have been published elsewhere.[36] It is no trivial matter to grow single crystals of pure gases at low temperatures, and it becomes much less so when the gases are mixtures or have a high concentration of impurities. The crystals were grown by maintaining a gradient of about 2.5 K between the top and the bottom clamp (with the top being warmer) and lowering the temperature by about 0.05—0.1 K per hour until a small (0.5-mm) seed formed on the bottom window. This was annealed for about one day. The annealing process increased the probability that the seed would display only one grain at the solid-liquid interface. After annealing, the seed was grown to a height of 1.5 mm, the growth rate varying between 0.05 and 0.1 mm h^{-1} with intermittent several-hour periods of constant temperature in which no growth took place. This was necessary so that any buildup of solute concentration at the solid-liquid interface was reduced by diffusion in the liquid and to a small extent in the solid.[50]

Transmission Laue x-ray diffraction photographs were then taken using a Philips (MG 101) x-ray source, a lead collimator, and a Polaroid XR-7 Land camera, with the film plane perpendicular to the Y axis (see Fig. 1) and 7.9 cm away from the cell. An exposure of about 2 min was sufficient to record the photographs. From these photographs it was initially determined whether the seed was of good quality and free of strain, whether it was polycrystalline, and whether the phase was fcc or hcp. The phase was further confirmed by studying the birefringence in these crystals. The procedure for finally establishing the phase of the crystal has been given in Ref. 36. Following successful completion of this procedure the crystal was grown to about 8 mm in height over a period of seven or eight days by the same slow growth procedure described above. The very slow growth rate ensured that quasiequilibrium conditions were maintained at all times, and allowed for sufficient annealing before further investigation.

From the positions of spots on the Laue photographs, the crystal orientation with respect to the laboratory frame of reference was determined in terms of Euler angles (θ,ϕ,χ).[51] This enabled the transformation of the sound wave vector $\vec{q}$ (which is known in the lab frame of reference because of the choice of scattering geometry) to the crystal Cartesian coordinates with respect to which the elastic constants are to be determined. The angle γ was then calculated from the relation

$$\cos\gamma = -q_y(\text{lab})\sin\theta\cos\phi + q_z(\text{lab})\cos\theta \ .$$

A least-squares-fitting procedure was used to calculate the final version of the rotation matrix and the Euler angles to within $\pm 0.5°$. Care was taken that each and every spot on the Laue photograph was taken into account in the orientation procedure. Once a particular orientation of the crystal was determined, then another orientation produced by rotation of the cell about the cryostat (Z) axis could easily be predicted (and least-squares fitted) because the rotation in question changed only the angle ϕ. Nevertheless, a slight wobble in the cell rotation also changed θ and χ, as noted in the results. A program written for the HP 9825 elec-

tronic calculator was used for the entire orientation procedure.[52]

C. Optics and spectrometer

The incident radiation was produced by a single-mode Ar^+ laser (Spectra Physics 165-08) at a wavelength of 514.5 nm. The laser beam, which was limited to 15 mW intensity by neutral density filters and always polarized perpendicular to the scattering plane (i.e., polarized along the X axis with reference to Fig. 1), was focused on the scattering volume by a quartz lens ($L1$) of focal length 25 cm. The laser beam was deflected upwards into the Z direction, through the cell, by a front surface mirror; the Y axis (scattering axis) was defined by a He-Ne laser beam. These two beams crossed at about 4 mm above the bottom clamp and defined the location of the scattering volume. The scattering angle was measured frequently with the help of an accurate pentaprism, and was normally set at $90°\pm15'$. The scattered light was restricted by an aperture ($A3$) to a cone of ~0.017 rad, and passed through a quartz collimating lens ($L2$) of 45-cm focal length before entering the Fabry-Perot interferometer. Light transmitted by the interferometer was focused on a 400-μm pinhole ($A4$) by a lens ($L3$) of 80-cm focal length, and was then focused onto the cathode of the cooled photomultiplier tube (ITT FW130).

With a multipassed Fabry-Perot interferometer, high finesse and extremely high contrast can be obtained at relatively small loss of intensity.[53] This allows for detection of signals which are extremely weak, relative to the central Brillouin component. The mirrors in the present interferometer were obtained from Burleigh Instruments, Inc., were dielectrically coated for a reflectivity of 93%, and were flat to $\lambda/200$ at 500 nm. The distance between the plates was measured with a traveling microscope, and two sets of free spectral ranges (FSR) of 10.50 and 4.00 GHz with a standard error of $\pm0.1\%$ were used. The observed minimum resolvable bandwidth of the spectrometer (the instrumental function) was 175 and 70 MHz for the two FSR's, respectively.

The output from the photomultiplier was coupled through an amplifier discriminator (PAR 1120) to a data acquisition and stabilization system (Burleigh DAS-1), which in turn provided the ramp voltage used in piezoelectrically scanning the Fabry-Perot (FP) interferometer. The same ramp also addressed, sequentially, the 1024 channels of the multichannel analyzer (MCA) memory, so that the channel number was directly proportional to the frequency shifts $\Delta\nu$ passed by the FP. Hence, spectral data were accumulated in the form of photon counts versus MCA channel number (or frequency of the scattered light). Additionally, the DAS-1 automatically compensates for frequency drifts due to both the laser and the FP, and utilized negative feedback circuitry to maintain parallel alignment of the FP mirrors for long periods of time (for details see Refs. 54 and 55). This allowed for arbitrarily long spectral accumulation times. Another important feature of the DAS-1 was the provision for spending more time in accumulating counts in selected regions of the spectrum. In this work, such regions were those where transverse components were expected to appear, and the region of the Rayleigh peak for stabilization purposes. The ramp could be made to spend between 1 and 99 more time units per channel in the segmented regions compared to normal. This greatly increased the effective signal-to-noise ratio capabilities. The DAS-1 is equipped with a cathode ray tube (CRT) screen so that spectral measurements could be made directly with the help of a cursor that identified the channel number and the accumulated number of counts. Usually only half of the MCA memory was used for recording the spectra, the accumulation time varying between 10 and 15 h. The other half was used to store and add the spectra obtained from several such runs. When sufficient signal-to-noise ratio was obtained, the spectrum was recorded by a strip chart recorder for permanent record.

III. EXPERIMENTAL RESULTS

A. Single crystals of hcp and fcc Ar doped with O_2 and N_2

As a result of considerable effort devoted to the development of the most appropriate techniques for crystal growth, a success rate of about one in three was realized for hcp crystals of $Ar(O_2)$, while for hcp $Ar(N_2)$ the success rate was somewhat less favorable. A number of (published[36]) conclusions were reached regarding the growth process, which appeared to be in conflict with the previously published phase diagrams.[28,30] In particular, and as already noted, at least $4\frac{1}{2}$ and 5 mol % of N_2 and O_2, respectively, were required (in the solid) in order to produce single crystals of the hcp phase under conditions of quasiequilibrium with the melt. Lower concentrations always yielded the fcc

structure.

An $Ar_{0.90}(O_2)_{0.10}$ gaseous mixture, which corresponds to about 6 mol % O_2 in the solid (as determined from the freezing point and the published diagram)[56] was found to give best results for growing hcp crystals. Seven cylindrical hcp $Ar(O_2)$ crystals were grown with dimensions 8 mm high and 3 mm in diameter. These crystals were clear, transparent, colorless, and without any visual defects and also exhibited birefringence when viewed through crossed polaroids. Several of the samples showed doubling of Laue spots at some orientations and were found to be twinned, with the difference in the Euler angles of the twins being within the limits of the experimental error ($\pm 0.5°$).

One fcc $Ar_{0.96}(O_2)_{0.04}$ and two fcc $Ar_{0.98}(O_2)_{0.02}$ crystals were also studied. These crystals were also clear, transparent, and colorless and produced excellent quality Laue diffraction patterns. There was no evidence of birefringence in these crystals. Table I lists the freezing temperature, concentration, density, and refractive index of all the crystals studied.

Because of the steepness of the solidus curve in the $Ar(N_2)$ phase diagram,[57] it was more difficult to grow single crystals of this alloy. It was finally determined that $Ar(N_2)$ crystals of acceptable quality could be produced by using an $Ar_{0.70}(N_2)_{0.30}$ gaseous mixture. The resulting N_2 concentration in the solid was estimated to be 5 mol %, and the crystal structure was usually fcc. However, the cubic phase appeared to be unstable at this particular concentraion, and on two occasions, an fcc-to-hcp phase transformation was observed (after growth was complete) to proceed downward from the top of the sample such that the lower (~ 2 mm) portion remained single-crystal fcc (no. NF1), whereas the upper portion was a slightly strained hcp crystal (no. NH1). This was established by analyzing the Laue diffraction photographs, and from the observed birefringence (see Ref. 36 for further details).

B. Brillouin spectra of single crystals of Ar alloys

1. hcp crystals

Brillouin spectra were recorded at various orientations of the seven hcp $Ar_{0.94}(O_2)_{0.06}$ crystals (nos. OH1–OH7), resulting in a total of 47 spectra, which yielded 79 frequency-shift measurements. Table II contains the Euler angles, the angle γ, and the observed longitudinal $\nu(L)$, and the fast $\nu(T_2)$ and slow $\nu(T_1)$ transverse frequency shifts. Crystals nos. OH1 and OH3 were destroyed because of power failures before any reasonable number of spectra could be recorded. In recording the spectra from various crystals, attempts were made to vary γ as much as possible. Data points at *small* and at *large* γ angles were necessary to find c_{33}, c_{11}, c_{12} precisely [see Eqs. (4)]. The range of γ values studied was between 25° and 90°. No crystals were obtained that could give values of γ below 25°, and would indeed be improbable geometrically. An example of a Brillouin spectrum from the hcp phase is shown in Fig. 3.

In all spectra, L components were always present, and T_2 components were usually observed. However, for the hcp $Ar(O_2)$ samples the slow transverse component T_1 was only observed twice in crystal no. OH7 when it was very weak. The central component was usually quite intense and was believed to be mainly due to parasitic scattering. The intensity of the T_2 component varied with the orientation of the crystal, and the average peak intensity ratio $I(T_2)/I(L)$ is plotted as a function of angle γ in Fig. 4. It shows that a minimum in this ratio occurs in the region between 50°–60°.

In the hcp $Ar_{0.95}(N_2)_{0.05}$ crystals, no T_1 components were observed, and the L and T_2 frequencies were slightly higher than those of hcp $Ar_{0.94}(O_2)_{0.06}$ crystals at the same γ. The data for this crystal are given in Table III and were considered insufficient for meaningful further analysis.

TABLE I. Physical data of experimental samples of Ar with impurities.

Crystal no.	Impurity in gas mixture	Temperature at freezing point (K)	Gradient ($K\,cm^{-1}$)	Temperature at scattering volume $T_s(K)$	Crystal structure	Average estimated impurity concentration in solid	Density at T_s ($g\,cm^{-3}$)	Refractive index at T_s and $\lambda=514.5$ nm
OF1 and OF2	5% O_2	83.3	1.2	83.0	fcc	2% O_2	1.618	1.2691
OF3	$7\frac{1}{2}$% O_2	82.7	1.0	82.2	fcc	4% O_2	1.613	1.2687
OH1–OH7	10% O_2	81.5	1.0	81.3	hcp	6% O_2	1.608	1.2684
NF1 and NH1	30% N_2	78.9	2.0	77.8	fcc and hcp	5% N_2	1.601	1.2689

TABLE II. Observed and calculated "best-fit" frequency shifts as a function of orientation for seven hcp $Ar_{0.94}(O_2)_{0.06}$ single crystals, at 81.3±0.3 K. The Euler angles and γ are given in degrees.

Crystal	Crystal orientation				Observed frequency shift (GHz)			Calculated frequency shift (GHz)		
no.	θ	ϕ	χ	γ	$\nu(L)$	$\nu(T_2)$	$\nu(T_1)$	$\nu(L)$	$\nu(T_2)$	$\nu(T_1)$
OH1	135.1	248.1	231.3	46.6	4.56			4.58	2.67	2.27
	135.3	239.2	231.4	40.8	4.64	2.61		4.62	2.65	2.26
	135.9	228.3	231.0	33.4	4.66	2.58		4.69	2.58	2.25
OH2	157.2	315.1	94.7	62.8	4.60			4.59	2.53	2.28
	157.1	295.7	95.3	57.9	4.55			4.57	2.59	2.28
	157.5	283.3	96.0	53.8	4.54			4.57	2.64	2.27
	156.1	252.9	97.1	43.1	4.58			4.60	2.66	2.26
	156.3	266.6	96.2	48.4	4.53			4.57	2.66	2.27
OH3	159.8	90.9	247.0	48.1	4.58			4.58	2.67	2.27
	160.0	67.9	244.8	55.0	4.55			4.57	2.62	2.28
OH4	165.0	170.6	95.1	30.4	4.74	2.53		4.74	2.55	2.25
	165.5	154.0	95.5	32.6	4.70	2.56		4.71	2.58	2.25
	166.3	141.0	97.4	35.3	4.69	2.61		4.68	2.61	2.26
	166.0	129.6	94.8	37.5	4.69	2.63		4.66	2.63	2.26
	165.8	118.9	94.1	39.8	4.65	2.64		4.64	2.65	2.26
	166.1	98.3	93.0	44.8	4.60	2.66		4.60	2.67	2.27
OH5	158.2	80.4	171.7	52.3	4.57			4.58	2.65	2.28
	157.6	75.3	171.8	54.3	4.58			4.58	2.64	2.28
	158.2	69.5	171.1	55.8	4.59			4.58	2.62	2.28
	157.7	64.4	171.2	57.6	4.58			4.58	2.60	2.28
	157.6	53.6	170.2	60.5	4.60	2.58		4.59	2.57	2.29
	157.5	43.1	169.6	63.0	4.60	2.53		4.60	2.53	2.29
	157.6	31.9	168.2	65.0	4.63	2.49		4.61	2.50	2.29
	156.9	13.8	168.0	67.8	4.62	2.45		4.62	2.46	2.30
	156.7	4.2	168.1	68.4	4.65	2.43		4.63	2.45	2.30
OH6	20.1	350.0	61.9	25.4	4.79	2.48		4.78	2.47	2.24
	20.0	340.7	61.3	26.8	4.78	2.51		4.77	2.49	2.24
	20.2	327.4	62.8	29.6	4.73	2.54		4.73	2.54	2.24
	20.1	330.0	62.1	29.0	4.74	2.55		4.74	2.53	2.24
	20.1	320.4	61.6	31.6	4.72	2.56		4.71	2.56	2.25
	20.4	299.9	62.1	38.2	4.64	2.63		4.64	2.63	2.25
	20.6	240.0	62.3	57.5	4.59	2.59		4.57	2.60	2.28
OH7	94.8	84.6	106.0	89.6	4.68			4.68	2.23	2.30
	94.9	88.7	105.9	87.5	4.68			4.68	2.23	2.30
	95.0	89.6	105.9	86.7	4.67	2.22		4.68	2.23	2.30
	95.0	93.6	105.7	83.9	4.68	2.26		4.68	2.25	2.30
	95.2	102.1	105.7	77.8	4.66			4.66	2.31	2.30
	94.8	114.5	105.6	69.4	4.63	2.45		4.62	2.42	2.29
	94.9	123.0	105.6	63.6	4.59	2.52		4.59	2.51	2.29
	95.0	133.2	105.8	57.1	4.58	2.61		4.57	2.60	2.28
	94.9	136.2	105.7	55.3	4.58			4.57	2.62	2.28
	95.1	140.1	105.7	52.9	4.57			4.57	2.64	2.27
	95.1	145.9	105.7	49.8	4.57	2.67	2.25	4.57	2.66	2.27
	95.1	153.1	105.6	46.3	4.59	2.70		4.58	2.67	2.27
	95.1	159.1	106.0	43.9	4.60	2.68		4.60	2.66	2.26
	95.1	160.1	105.8	43.5	4.60	2.66	2.28	4.60	2.66	2.26
	95.1	170.8	105.8	40.7	4.61	2.65		4.62	2.65	2.26

2. *fcc crystals*

In fcc $Ar_{0.98}(O_2)_{0.02}$ (nos. OF1 and OF2) and $Ar_{0.96}(O_2)_{0.64}$ (no. OF3) crystals, all three Brillouin components were observed at several orientations, and at others, either T_2 was present together with L, or only the latter was present alone. Tables IV

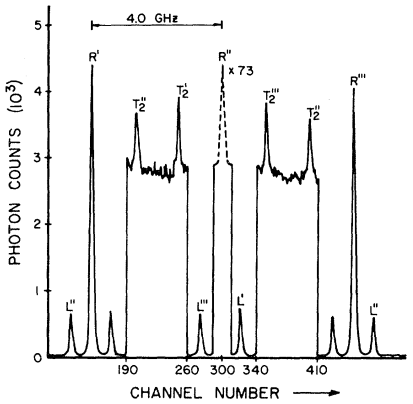

FIG. 3. Brillouin spectrum from a hcp $Ar_{0.94}(O_2)_{0.06}$ single crystal (OH7) at $\gamma=40.7°$. The spectrum was recorded in about 12 h with a laser power of 15 mW. The straight vertical lines indicate the regions in which the segmented ramp feature of the DAS-1 was used. Fast transverse components T_2 and the longitudinal components are marked with primes to indicate the central peak (R) order to which they belong. Peak intensity ratio of $L:R=1:7$ and of $T_2:L=1:50$. This represents a T_2 intensity of about 4 counts sec^{-1}.

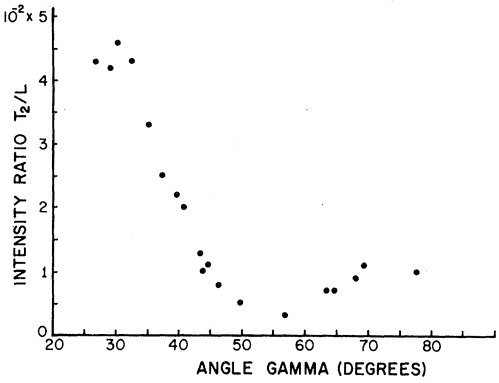

FIG. 4. Observed variation of intensity of the fast transverse component T_2, in the hcp $Ar_{0.94}(O_2)_{0.06}$ single crystals is plotted as a ratio T_2/L vs the angle γ.

and V contain the Euler angles and the observed frequency shifts for these fcc crystals. An example of a spectrum from the fcc phase is shown in Fig. 5.

In the case of the fcc $Ar_{0.95}(N_2)_{0.05}$ crystal (no. NF1), 20 spectra were recorded, giving 47 frequency-shift measurements; these are listed in Table VI. In this particular crystal, all three components were frequently observed, with their relative intensities varying markedly with orientation. An interesting qualitative observation was the fact that in a fcc Ar alloy crystal the light beam appeared, by eye, to be more intense than in a hcp crystal in all the orientations. This was clearly apparent in the case of $Ar(N_2)$ crystals where both hcp and fcc phases were present at different heights.

C. Elastic constants and error analysis

In order to calculate the elastic constants from the observed frequency shifts (ν^{obs}), values for the density ρ and refractive index n of the sample were required. These were calculated by the procedures outlined in Appendixes A and B and are given in Table I.

The elastic constants were calculated from ν^{obs}, by using an iterative procedure utilizing an IBM 370/158 computer. In the case of hcp crystals, initial values of all the five elastic constants c_{11}, c_{12}, c_{13}, c_{33}, and c_{44} were assumed, and the three sound velocities $V_\mu(\vec{q})$ were calculated for each orientation of the crystal from Eq. (4). These velocities were then used to calculate the frequencies of the three modes from Eq. (1). In each cycle of itera-

TABLE III. Observed and calculated "best-fit" frequency shifts as a function of orientation for one hcp $Ar_{0.95}(N_2)_{0.05}$ crystal at 77.8±0.3 K. The Euler angles and γ are given in degrees.

Crystal	Crystal orientation				Observed frequency shift (GHz)			Calculated frequency shift (GHz)		
no.	θ	ϕ	χ	γ	$\nu(L)$	$\nu(T_2)$	$\nu(T_1)$	$\nu(L)$	$\nu(T_2)$	$\nu(T_1)$
NH1	11.4	223.4	14.6	53.7	4.64	2.69		4.64	2.68	
	11.7	194.6	13.5	56.4	4.65			4.65	2.66	
	12.1	174.8	13.5	57.1	4.66	2.65		4.66	2.65	
	11.9	166.6	11.5	56.6	4.66	2.66		4.65	2.65	
	11.9	144.7	11.8	55.0	4.64			4.65	2.67	
	12.0	129.6	12.4	53.3	4.64			4.64	2.68	
	11.8	107.5	11.1	49.6	4.63	2.71		4.63	2.70	
	11.5	98.3	10.8	47.7	4.64	2.70		4.63	2.71	

TABLE IV. Observed and calculated "best-fit" frequency shifts as a function of orientation for two fcc $Ar_{0.98}(O_2)_{0.02}$ single crystals at 83.0±0.3 K. The Euler angles are given in degrees.

Crystal	Crystal orientation			Observed frequency shift (GHz)			Calculated frequency shift (GHz)		
no.	θ	ϕ	χ	$\nu(L)$	$\nu(T_2)$	$\nu(T_1)$	$\nu(L)$	$\nu(T_2)$	$\nu(T_1)$
OF1	129.6	106.4	334.0	4.79		1.84	4.81	2.87	1.84
	129.6	96.0	334.1	4.75	2.81	2.00	4.76	2.83	2.01
	129.8	86.7	334.0	4.71	2.76	2.17	4.71	2.77	2.18
	129.7	77.2	334.0	4.67		2.31	4.68	2.72	2.32
	129.9	67.4	333.9	4.69	2.74	2.29	4.68	2.74	2.29
	129.7	57.7	333.9	4.72	2.81	2.14	4.71	2.81	2.14
	129.5	47.4	334.1	4.76		1.96	4.76	2.87	1.95
	129.7	37.9	333.9	4.80		1.81	4.80	2.88	1.81
	129.5	27.9	334.1	4.83			4.83	2.88	1.75
	129.4	23.0	334.0	4.82		1.77	4.82	2.88	1.77
	129.5	18.0	334.1	4.81		1.82	4.81	2.87	1.81
	129.5	358.2	334.4	4.66		2.21	4.64	2.86	2.22
	129.5	353.0	334.3	4.56		2.39	4.58	2.86	2.36
	129.5	348.1	334.3	4.51		2.48	4.51	2.86	2.48
	129.2	338.6	334.4	4.35		2.69	4.37	2.87	2.71
OF2	94.1	201.3	104.5	4.95	2.45	2.00	4.96	2.47	2.01
	94.1	191.7	104.4	4.90	2.63	1.92	4.90	2.64	1.92
	94.2	181.0	104.2	4.85	2.80	1.83	4.85	2.80	1.83
	94.3	171.0	104.4	4.82		1.78	4.82	2.88	1.77
	94.2	161.4	104.2	4.83			4.83	2.88	1.76
	94.2	151.1	104.2	4.86	2.81	1.81	4.86	2.80	1.80
	94.2	141.2	104.3	4.89	2.69	1.91	4.88	2.69	1.90
	94.4	131.3	104.4	4.90	2.59	2.00	4.89	2.58	2.02
	94.2	116.4	104.2	4.88	2.59	2.11	4.86	2.58	2.10
	94.2	101.2	104.1	4.80	2.79	2.01	4.78	2.78	2.02
	94.1	81.4	104.1	4.74	2.88	2.00	4.73	2.88	2.01
	93.9	71.1	104.1	4.74	2.80	2.08	4.75	2.79	2.08

TABLE V. Observed and calculated "best-fit" frequency shifts as a function of orientation for a fcc $Ar_{0.96}(O_2)_{0.04}$ single crystal, at 82.2±0.3 K. The Euler angles are given in degrees.

Crystal	Crystal orientation			Observed frequency shift (GHz)			Calculated frequency shift (GHz)		
no.	θ	ϕ	χ	$\nu(L)$	$\nu(T_2)$	$\nu(T_1)$	$\nu(L)$	$\nu(T_2)$	$\nu(T_1)$
OF3	23.9	105.6	154.0	4.77	2.81	1.87	4.79	2.83	1.88
	23.9	96.8	153.7	4.78		1.79	4.79	2.87	1.80
	23.7	86.6	153.9	4.81	2.87	1.75	4.82	2.85	1.76
	23.6	77.8	153.9	4.85	2.78	1.79	4.85	2.78	1.78
	23.9	67.7	153.8	4.87	2.69	1.88	4.87	2.69	1.87
	23.6	58.3	153.9	4.85	2.62	2.00	4.86	2.61	2.00
	23.6	48.7	153.8	4.82		2.13	4.82	2.59	2.13
	23.6	40.4	153.8	4.76	2.62	2.18	4.77	2.64	2.18
	23.5	32.2	153.8	4.70	2.74	2.20	4.70	2.74	2.20
	23.6	22.2	154.0	4.64	2.84	2.22	4.63	2.84	2.23
	23.6	12.3	153.9	4.59		2.28	4.58	2.87	2.28
	23.6	2.9	153.6	4.59	2.82	2.36	4.48	2.82	2.36
	23.5	352.9	153.5	4.61		2.41	4.59	2.75	2.41
	23.2	342.5	153.8	4.63	2.76	2.34	4.63	2.75	2.33

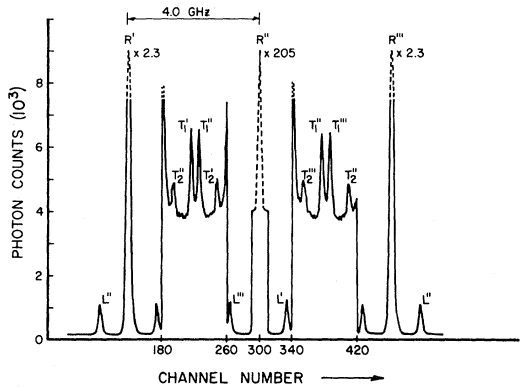

FIG. 5. Brillouin spectrum from a fcc $Ar_{0.96}(O_2)_{0.04}$ single crystal (OF3) at orientation ($\theta=23.9°$, $\phi=67.7°$, $\chi=153.8°$). The spectrum was recorded in about 15 h with a laser power of 15 mW. Straight vertical lines indicate the regions in which the segmented ramp feature of the DAS-1 was used. Components are marked with primes to indicate the central peak (R) order to which they belong. Peak intensity ratio of $L:R=1:21$, $T_1:L=1:30$ and $T_2:L=1:75$. This represents T_1 and T_2 intensities of about 4 and 2 counts sec^{-1}, respectively.

tion, the computer program calculated sets of mode frequencies corresponding to all the different crystal orientations specified by the Euler angles. The differences between the calculated and the measured frequency shifts were minimized by a least-squares-fitting procedure based on Newton's method, which is discussed in detail elsewhere.[58] In brief, this involved minimizing the squared error term χ^2 with respect to the variation of the elastic constants c_{ij}:

$$\chi^2(c_{ij})=\frac{1}{D}\sum_{K=1}^{N}\left[\frac{\nu_K^{\text{calc}}(c_{ij})-\nu_K^{\text{obs}}}{\sigma_K}\right]^2. \tag{9}$$

Here N is the total number of frequency shifts used in the determination of the elastic constants, D is the number of degrees of freedom, and σ_K is a weighting factor representing the estimated standard deviation of the Kth frequency-shift measurement, which was taken to be 0.015 GHz. Those c_{ij}'s that minimized χ^2 were taken as the "best-fit" elastic constants. The values for various hcp $Ar_{0.94}(O_2)_{0.06}$ crystals are given in Table VII. The relative consistency in the values of the elastic constants calculated from different single crystals grown is evident. It was not possible to calculate c_{12} in crystal nos. OH1—OH6, since it appears only in the equation for the T_1 component [see Eq. (4)], which was not observed. T_1 components *were* observed in crystal OH7, hence all five elastic constants could be calculated independently for this

TABLE VI. Observed and calculated "best-fit" frequency shifts as a function of orientation for a fcc $Ar_{0.95}(N_2)_{0.05}$ single crystal at 77.8±0.3 K. The Euler angles are given in degrees.

Crystal	Crystal orientation			Observed frequency shift (GHz)			Calculated frequency shift (GHz)		
no.	θ	ϕ	χ	$\nu(L)$	$\nu(T_2)$	$\nu(T_1)$	$\nu(L)$	$\nu(T_2)$	$\nu(T_1)$
NF1	92.0	157.8	88.2	4.91	2.63		4.92	2.63	1.88
	91.8	148.7	88.0	4.96	2.48	2.00	4.97	2.48	1.98
	92.0	138.5	88.3	5.00	2.34	2.07	4.99	2.34	2.08
	91.8	129.2	88.1	5.00	2.35	2.07	4.99	2.36	2.06
	91.8	119.3	88.2	4.97	2.49	1.98	4.96	2.51	1.95
	92.1	107.6	88.3	4.90	2.69		4.90	2.69	1.85
	92.4	99.2	88.4	4.88			4.87	2.79	1.80
	92.2	96.7	88.3	4.86	2.83	1.80	4.86	2.82	1.79
	92.0	88.9	88.4	4.85		1.76	4.84	2.85	1.77
	92.1	84.1	88.3	4.85			4.84	2.84	1.78
	91.6	78.1	88.3	4.88	2.82		4.86	2.80	1.79
	91.8	72.5	88.4	4.87			4.88	2.75	1.82
	91.8	67.4	88.3	4.91	2.68	1.86	4.91	2.68	1.86
	91.8	62.1	88.4	4.92		1.90	4.93	2.60	1.90
	92.2	57.1	88.1	4.94	2.52	1.95	4.95	2.53	1.95
	92.0	52.2	88.5	4.97		2.00	4.96	2.46	2.01
	91.6	51.2	88.5	4.96	2.44	2.01	4.97	2.43	2.02
	92.2	48.0	87.8	4.98	2.40	2.05	4.97	2.41	2.04
	91.9	40.4	88.3	4.96		2.07	4.98	2.38	2.07
	91.8	32.8	88.3	4.96	2.47	2.00	4.96	2.46	2.01

TABLE VII. Adiabatic elastic constants and bulk modulus (units: 10^9 N m^{-2}) of hcp $Ar_{0.94}(O_2)_{0.06}$ single crystals at $T=81.3\pm0.3$ K as determined in this work.

Crystal no.	No. of frequency shifts N	Elastic constants c_{11}	c_{12}	c_{13}	c_{33}	c_{44}	Bulk modulus B_S
OH1, OH2, and OH3[a]	12	2.88		1.19	3.20	0.648	
		(2.88)	(1.51)	(1.19)	(3.20)	(0.648)	(1.86)
OH4 and OH5[a]	26	2.91		1.20	3.25	0.648	
		(2.91)	(1.54)	(1.20)	(3.25)	(0.648)	(1.88)
OH6[a]	14	2.89		1.19	3.23	0.679	
		(2.89)	(1.52)	(1.19)	(3.23)	(0.679)	(1.86)
OH7[b]	27	2.90	1.51	1.17	3.26	0.660	1.87
		(2.91)	(1.52)	(1.17)	(3.25)	(0.661)	(1.87)
All seven[b] crystals	79	2.90	1.50	1.18	3.24	0.656	1.86
		(2.90)	(1.52)	(1.18)	(3.24)	(0.657)	(1.87)

[a]Since the T_1 component was not observed in these crystals, c_{12} could not be independently calculated. The values given in parentheses are those obtained by assuming the relation $c_{12}=c_{13}+c_{11}-c_{33}$.

[b]All five elastic constants were calculated, treating each as an independent variable.

crystal. With c_{ij} values it was found that $c_{11}+c_{12}-c_{13}-c_{33}=0$ holds true within experimental error and essentially indicates that the c/a ratio is independent of pressure.[59] Using this relation, all the five elastic constants for crystal nos. OH1—OH6 could be calculated and are given in parentheses in Table VII.

The final values of the elastic constants of $Ar_{0.94}(O_2)_{0.06}$ single crystals (all c_{ij}'s treated as independent variables) at 81.3 ± 0.3 K were determined as (units 10^9 N m^{-2})

$$c_{11}=2.90\pm0.04\ ,\quad c_{33}=3.24\pm0.05\ ,$$

$$c_{12}=1.50\pm0.03\ ,\quad c_{44}=0.65(6)\pm0.011\ ,$$

$$c_{13}=1.18\pm0.02\ ,$$

where the uncertainties in c_{ij}'s shown are discussed below. The frequency shifts (and velocities) calculated from these final values of the c_{ij}'s are plotted as a function of angle γ in Fig. 6 (indicated by solid curves) along with the experimental data points. The same fitting procedure was used for calculating the fcc elastic constants c_{11}^F, c_{12}^F, and c_{44}^F, using Eq. (2). The best values of the fcc elastic constants of $Ar_{0.98}(O_2)_{0.02}$, $Ar_{0.96}(O_2)_{0.04}$ and $Ar_{0.95}(N_2)_{0.05}$ are given in Table VIII, which also contains the adiabatic bulk modulus and the elastic anisotropy factor A for these crystals.

There are two categories of possible errors in the elastic constants. The first category concerns the *relative* values of the c_{ij}'s, and for hcp $Ar_{0.94}(O_2)_{0.06}$ cyrstals the uncertainties are $\pm0.2\%$ in c_{11}, $\pm0.7\%$ in c_{12} ($\pm1.7\%$ with five-parameter fit), $\pm0.4\%$ in c_{13}, $\pm0.3\%$ in c_{33}, and $\pm0.6\%$ in c_{44}, as determined via the least-squares-fitting procedure. This *relative* uncertainty arises from a combination of the uncertainties in the measurement of the Brillouin frequency shifts and the crystal-orientation determination. The second category of uncertainty concerns possible systematic errors in the spectral free range of the interferometer ($\pm0.1\%$), the scattering angle θ ($\pm0.3°$), the density ρ, and the refractive index n of the crystal. All these quantities appear as common factors in the expressions from which the elastic constants are calculated, and consequently change

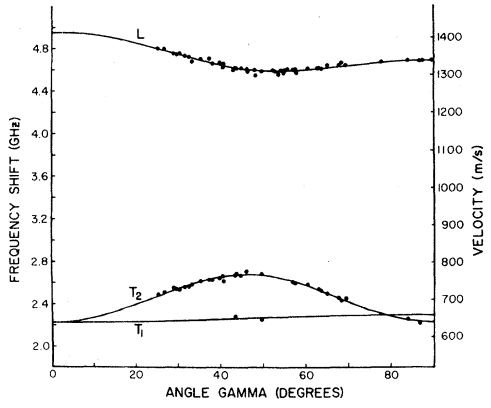

FIG. 6. Variation of frequency shifts and the sound velocity as a function of angle γ between the c axis and the direction of sound propagation in hcp crystals of $Ar_{0.94}(O_2)_{0.06}$ at 81.3 ± 0.3 K. Solid dots are the experimental data points, and the solid curves calculated from the final values of the elastic constants.

TABLE VIII. The adiabatic elastic constants, bulk modulus B_S (both in units of 10^9 N m^{-2}), and anisotropy factor A of fcc Ar single crystals doped with various percentages of O_2 and N_2.

Elastic constants	Pure Ar[a] 82.3 K	2% O_2 83.0 K	4% O_2[b] 82.2 K	5% N_2[c] 77.8 K
c_{11}	2.38±0.04	2.40±0.03	2.39±0.03	2.43±0.05
c_{12}	1.56±0.03	1.58±0.02	1.59±0.02	1.61±0.04
c_{44}	1.12±0.03	1.11±0.02	1.09±0.02	1.07±0.03
B_S	1.83±0.03	1.85±0.02	1.86±0.02	1.88±0.03
A	2.73±0.1	2.71±0.06	2.73±0.06	2.61±0.07

[a]Pure Ar values taken from Ref. 72.
[b]Concentrations of $O_2 \gtrsim 4\%$ gave rise to the hcp structure.
[c]Crystals of acceptable quality could not be obtained for N_2 concentrations $\gtrsim 5\%$.

the absolute values of the c_{ij}'s by the same ratio. ρ and n were determined by procedures outlined in Appendixes A and B. The uncertainty in these arise from three possible contributions. The first is the accuracy with which the concentration of solute was determined from the published phase diagrams. Concentration was estimated to ±1% (absolute), resulting in an uncertainty of ±0.2% in ρ and ±0.03% in n. Secondly, the published phase diagrams[31] themselves have an estimated uncertainty of about ±1% (absolute) in concentration, corresponding to ±0.5 K. Thirdly, the pure density has an uncertainty of about ±0.1%,[27] and n for Ar, O_2, and N_2 has about ±0.1%.[60,61] An additional uncertainty of ±0.1% was added to n to represent the maximum variation in n at the relevant wavelength and temperature range. Thus the total estimated uncertainties in ρ and n are ±0.5% and ±0.3%, respectively. The possible *systematic* error in each of the elastic constants is therefore approximately ±1%.

As a result, the total *absolute* uncertainty in all the c_{ij}'s is estimated to be well within ±2%. The same error analysis applies to $Ar_{0.98}(O_2)_{0.02}$ and $Ar_{0.96}(O_2)_{0.04}$ elastic constants. Because of the relatively high uncertainty in the concentration of N_2 the total error in fcc $Ar_{0.95}(N_2)_{0.05}$ is estimated to be within 2.5%.

IV. DISCUSSION

The following discussion attempts to isolate the most interesting and potentially significant features of the foregoing results by a process of comparison among the different samples involved, as well as by utilizing available information for pure Ar and other simple molecular solids. Recent observations and interpretation of the (pure) vibrational Raman spectra for the alloy samples in question[62,63] provide the basis for an assumption which is made throughout the discussion, namely, that the O_2 and N_2 solute molecules occupy substitutional sites in the Ar lattice.

A. Rotation-translation coupling in van der Waals solids

The isoelectronic materials β-N_2 and β-CO are among the few simple molecular solids of hcp structure for which elastic constant data are available.[64,65] A comparison with the elastic properties of hcp $Ar_{0.94}(O_2)_{0.06}$ (see Table IX) reveals the following points of similarity. (1) The c_{ij}'s for β-N_2 and β-CO are very similar, but somewhat lower in magnitude than those of hcp $Ar_{0.94}(O_2)_{0.06}$, (2) the requirements for elastic isotropy [i.e., $A = c_{11}/c_{33} = (c_{11}+c_{12})/(c_{13}+c_{33}) = 1$] are very nearly satisfied in each case, and (3) the variations of frequency shift (or velocity) versus the angle γ are qualitatively similar for all three solids (in contrast to, say, the case[66] for para-H_2).

The Cauchy ratios c_{13}/c_{44} however, are considerably greater than the value of unity expected for isotropic intermolecular interactions and have significantly different values for each of the three materials. This indicates that anisotropic contributions to the interaction potential are of (varied) importance, and in the case of the Ar(O_2) mixture, the effect is clearly impurity related since the values of c_{13}/c_{44} were found to consistently increase with increasing concentration of O_2 (and N_2; see Table X). This is taken to indicate that there is a significant interaction between the host lattice and reorientational (rotational) motion of the diatomic impurities (i.e., rotation-translation coupling). Again, in the case of the Ar alloy this is

TABLE IX. The adiabatic elastic constants and bulk modulus (units: 10^9 N m^{-2}) and their various ratios for the hcp van der Waals lattices.

Substance	T (K)	c_{11}	c_{12}	c_{13}	c_{33}	c_{44}	c_{66}[d]	B_S	A[e]	$\frac{c_{11}}{c_{33}}$	$\frac{c_{11}+c_{12}}{c_{13}+c_{33}}$	$\frac{c_{13}}{c_{44}}$
β-N_2[a]	63.0	1.825	1.131	0.980	1.976	0.320	0.347	1.31	0.92	0.92	1.0	3.06
β-CO[b]	67.7	1.901	1.146	0.951	2.095	0.355	0.378	1.33	0.94	0.91	1.0	2.68
$Ar_{0.94}(O_2)_{0.06}$[c]	81.3	2.90	1.50	1.18	3.24	0.656	0.70	1.87	0.94	0.90	$\sim$1.0	1.80

[a]Reference 64.
[b]Reference 65.
[c]Present work.
[d]$c_{66}=\frac{1}{2}(c_{11}-c_{12})$, shear modulus.
[e]$A=2c_{44}/(c_{11}-c_{12})$.

supported in an important way by recent observations (in this laboratory[67]) of the low-frequency Raman spectra in single crystals of $Ar(O_2)$, $Ar(N_2)$, and Ar(CO). Readily identifiable features in these spectra were associated (1) with the reorientation of solute molecules and (2) with impurity-induced lattice vibrations in the Ar host. Although these effects are not very pronounced, and indeed may be of negligible significance in most other contexts, it is of obvious importance here to consider the possibility that they may play a key role in determining the phase of a given Ar alloy where such a delicate balance between the two possible structures is known to exist. In fact, it is clearly relevant to note that, whereas most of the physical properties of β-N_2 and β-CO are very closely similar, there is a marked difference between the α-β transition temperatures for each (35.6 and 61 K, respectively), which may be correlated with the anomalous difference between the Cauchy ratios already noted, in this case, probably due to fluctuations in orientational ordering (see also Ref. 65).

The question of the relative importance of the rather subtle reorientational effects and the manner in which they are manifested have received some attention in the literature. For example, calculations by Klein and Weis[68] were found to be in disagreement with the β-N_2 transverse-mode data by more than a factor of 2,[65] and they concluded that the anomalously low (experimental) transverse velocities indicated strong coupling to the orientational motion of the molecules (see also Ref. 69). Independently, the effect of rotation-translation coupling was calculated to lower the sound velocities in ordered α-N_2.[70] Also, Rand and Stoicheff,[71] in recent Brillouin measurements, identified an anomalously "slow" T_1 mode in the $\langle 110 \rangle$ crystalline direction of methane by comparing all three acoustic modes of CH_4 and CD_4 with those of the rare-gas solids, and thereby confirmed the effect in question.

There is, consequently, a rather broad base of support for the importance of the rotation-translation coupling mechanism in van der Waals solids. The remainder of the discussion in this section will serve to emphasize this point while providing further supporting arguments.

TABLE X. The adiabatic elastic constants of hcp $Ar_{0.94}(O_2)_{0.06}$ single crystals and the fcc values of argon and its alloys transformed to trigonal and hcp structure (units: 10^9 N m^{-2}).

Elastic constants	Experimental (c_{ij}) hcp $Ar_{0.94}(O_2)_{0.06}$ 81.3 K	Trigonal ($\bar{c}_{ij}$) Pure Ar 82.3 K	2% O_2 83.0 K	4% O_2 82.2 K	5% N_2 77.8 K	Hexagonal (c_{ij}^H) Pure Ar 82.3 K	2% O_2 83.0 K	4% O_2 82.2 K	5% N_2 77.8 K
c_{11}	2.90±0.04	3.09	3.10	3.08	3.09	2.92±0.04	2.93±0.4	2.91±0.04	2.94±0.06
c_{12}	1.50±0.03	1.32	1.35	1.36	1.39	1.50±0.03	1.52±0.02	1.53±0.02	1.54±0.04
c_{13}	1.18±0.02	1.09	1.11	1.13	1.17	1.09±0.02	1.11±0.02	1.13±0.02	1.17±0.03
c_{33}	3.24±0.05	3.34	3.33	3.31	3.31	3.34±0.05	3.33±0.04	3.31±0.04	3.31±0.07
c_{44}	0.656±0.01	0.647	0.643	0.630	0.630	0.647±0.02	0.634±0.01	0.630±0.10	0.630±0.015
c_{14}	0.0	−0.335	−0.330	−0.325	−0.311	0.0	0.0	0.0	0.0
c_{13}/c_{44}	1.80±0.02					1.68±0.02	1.73±0.02	1.79±0.02	1.86±0.03

B. Elastic constants of Ar and Ar(X_2)

1. *fcc structure*

The fcc elastic constants of pure Ar have been determined using several different experimental techniques,[72–76] but (for various reasons[72]) the results do not all agree within the quoted error limits. The Brillouin scattering data of Gewurtz and Stoicheff[72] have been chosen for purposes of comparison with this work because of the common techniques employed.

With reference to Table VIII, it must first be pointed out that the elastic constants for $Ar_{0.95}(N_2)_{0.05}$ correspond to a significantly lower (freezing) temperature than the other listings. On the basis of previously published work[72,77] it is expected that a decrease in temperature from 82 to 78 K for pure Ar should give rise to *increases* of about 6% for both c_{11} and c_{44} and 5% for c_{12}. Assuming only that the corresponding behavior for Ar(X_2) mixtures is qualitatively the same, the following observations can be made regarding Table VIII. Given the quoted errors, the first three entries for c_{11} (which correspond to approximately the same temperature) show no significant trend that can be identified with the increasing impurity concentration. Likewise, the overall increase ($\sim 2\%$) for the 5% N_2 case cannot properly be regarded as significant, and even if it were to be regarded as such, it could most reasonably be associated with the temperature dependence referred to above. Similar comments apply to the c_{12} values, except that an overall consistent trend is apparent. For c_{44}, however, the trend is opposite to that expected from the temperature dependence and, even if the (liberal) error limits are strictly applied, only a minor correction for the latter effect would give rise to a significant overall *decrease* associated with the addition of 5% N_2. It should now be recalled that the structure of the $Ar_{0.95}(N_2)_{0.05}$ crystal was observed to be unstable, with both the fcc (no. NF1) and hcp (no. NH1) phases eventually being observed in the same sample (Sec. III A). It is therefore reasonable to assume that this instability is reflected in the c_{44} shear constant as a mode-softening effect. The slight decrease of c_{44} with increasing O_2 concentration is then consistent with with increasing instability of the fcc phase (see also Table X). As previously discussed, the most probable mechanism is one of coupling between the reorientational motion of the impurity molecules and the acoustic shear waves. The proposition that the phase of these mixed crystals can actually be determined by this coupling mechanism is consequently given added support. Rotation-translation coupling can certainly constitute the driving mechanism of phase transitions in more complex materials, such as ammonium bromide.[78]

With respect to theoretical calculations, it has already been noted that no attempt has (previously) been made to calculate the elastic constants of doped Ar crystals. Considerable effort, however, has been devoted to the determination of realistic potentials, and to the application of Monte Carlo techniques in the calculation of c_{ij}'s for pure fcc Ar.[77,79–84] A comparative review of the theoretical anf experimental values has been presented by Gewurtz and Stoicheff,[72] and a corresponding listing comprises part of Table XI. Extremely good agreement with experimental values [including those for fcc $Ar_{0.98}(O_2)_{0.02}$ presented here] is obtained when the three-body triple-dipole term as given by Axilrod, Teller, and Muto (ATM) is included in the Parson-Siska-Lee (PSL) potential.

2. *hcp structure*

The only available experimental data pertaining to the elastic constants of hcp Ar are presented in this paper. Fortunately, however, comparisons with c_{ij} data for the fcc phase are made possible by application of the methods of Sec. I B. As shown on Table X, the fcc values (c_{ij}) are first transformed into ($\bar{c}_{ij}$) values corresponding to an intermediate trigonal representation, and then converted to hcp values (c_{ij}^H) by assuming the existence, in general, of two internal strains. These strain corrections for pure Ar were

$$I_1 = 0.174, \quad I_2 = 0.127$$

in units of $10^9\ \mathrm{N\,m^{-2}}$. I_1 affected only the values of c_{11}^H and c_{12}^H, and gave rise to improved agreement with the corresponding experimental values for hcp $Ar_{0.94}(O_2)_{0.06}$. c_{13}^H and c_{33}^H were strain-free. I_2 affected only the value of c_{44}^H, but gave rise to less favorable agreement with the experimental c_{44} [for hcp $Ar_{0.94}(O_2)_{0.06}$]. I_2 was consequently set equal to zero without further justification, although similar conclusions were reached by Leamy and Warlimont[46] for fcc-hcp metallic structures and by Goldman[85] for calculations on the effects of internal strain on elastic constants of hcp H_2 and D_2. While this may compromise the significance of any comparisons involving c_{44}^H values with the experimental values, it is presumed to be of little consequence here since the emphasis in what

TABLE XI. Computed and experimental values of the fcc elastic constants of Ar (near 80 K in units of 10^9 N m^{-2}) and the same values transformed to hcp structure.

		T	fcc				hcp				
	Ref.	(K)	c_{11}	c_{12}	c_{44}	A	c_{11}^H	c_{12}^H	c_{13}^H	c_{33}^H	c_{44}^H
Theoretical											
MLJ (12-6)[a]	79	80	2.31	1.53	1.20	3.10	2.90	1.48	0.99	3.39	0.660
BB[b] and ATM[c]	79	80	2.50	1.62	1.18	2.70	3.06	1.55	1.13	3.48	0.687
BFW[d] and ATM	77	80	2.48	1.65	1.12	2.70	3.02	1.59	1.18	3.42	0.650
PSL[e] and ATM	80	80	2.37	1.57	1.12	2.80	2.91	1.51	1.09	3.33	0.640
Aziz[f] (fcc)	34,35	82	2.348	1.391	1.218	2.55	2.920	1.312	0.898	3.334	0.725
Aziz[f] (hcp)	34,35	82					2.946	1.312	0.876	2.874	0.763[h]
Experimental											
Ultrasonic	73	82	2.81	1.57	0.56	0.90	2.75	1.59	1.61	2.73	0.60
measurements	74	80	2.70	1.39	0.89	1.36	2.92	1.33	1.23	3.01	0.733
Neutron scattering	75	82	2.48	1.53	1.24	1.81	3.07	1.45	1.02	3.50	0.730
Stimulated Brillouin scattering	76	80	2.77	1.16	1.12	1.39	3.06	1.08	0.95	3.19	0.910
Brillouin scattering	72	82.3	2.38	1.56	1.12	2.73	2.92	1.50	1.09	3.33	0.647
Present results[g]		81.3					2.90	1.50	1.18	3.24	0.656[h]

[a]Mie-Lennard-Jones (12-6) potential.
[b]Bobetic-Barker potential.
[c]Axilrod-Teller-Muto triple-dipole interaction.
[d]Barker-Fisher-Watts potential.
[e]Parson-Siska-Lee potential.
[f]Calculations of Goldman and Klein using Aziz and Chen potential.
[g]For hcp $Ar_{0.94}(O_2)_{0.06}$.
[h]These are c_{ij}, not c_{ij}^H.

follows is on the intercomparison of transformed values only, where this particular elastic constant is concerned.

Referring again to Table XI, it can be seen that the best overall agreement between the theoretical c_{ij}^H values for pure Ar and the experimental values [for hcp $Ar_{0.94}(O_2)_{0.06}$] is obtained, as in the fcc case, for the PSL and ATM calculations. However, a significant anomaly occurs in the case of c_{13}^H, which differs by about 8% from the experimental value. There is also a consistent decrease in c_{13}^H with decreasing O_2 concentration, while the trend for c_{44}^H values is in the opposite sense. The result, as noted earlier in this section, is an enhanced and significant dependence of the Cauchy ratio c_{13}/c_{44} in O_2 concentration.

Attention is now drawn to the recent work of Goldman and Klein[34] (GK) (some of which is unpublished) which represents the only case where elastic constant calculations have been carried out for *both* the fcc and hcp phases of pure Ar. These results thus permit another, and perhaps more meaningful, level of comparison between experiment and theory that involves only the *differences* between the (direct) hcp values and the transformed fcc values in each case.

The condition assumed by GK were very close to the experimental ones, namely, a temperature of 82 K and a density corresponding to an fcc lattice constant of 0.546 nm. The intermolecular potential used was that of Aziz and Chen,[35] and the results were presented as a set of (elastic) parameters H_{ijkl} that were determined for the fcc structure in two approximations: (i) the self-consistent harmonic approximation and (2) the first-order self-consistent approximation.[86] For this work, these results were converted to the corresponding isothermal elastic constants c_{ij}^T with internal strain corrections included,[69,87] and the adiabatic elastic constants were then found via[88]

$$c_{11}=c_{11}^T+\Delta c,\quad c_{12}=c_{12}^T+\Delta c,\quad c_{44}=c_{44}^T\ , \tag{10}$$

where $\Delta c=\gamma^2 TC_v/V$, C_v is the specific heat at constant volume,[79] V the molar volume, and γ the Grüneisen constant.[77] In the case of the hcp structure, GK provided calculated values of the c_{ij}^T's in each of the phonon approximations referred to above, both with and without the internal strain corrections. These were again converted to the

corresponding adiabatic values through relations similar to Eqs. (10).[88]

The results of GK's calculations using the first-order self-consistent phonon theory are included in Table XI where the transformed fcc-to-hcp values are also shown in order to permit a *structural* comparison. Internal strain was included in both the transformation procedure and in the direct calculation of hcp values. The most significant point to note is that in spite of reasonable overall agreement with experimental values, the *differences* between the experimental c_{ij}^{H} values (for pure Ar) and the corresponding values for hcp $Ar_{0.94}(O_2)_{0.06}$ are not accounted for. There is only a small difference ($\sim 2.5\%$) between the theoretical c_{13} values, and it is opposite in sense to that observed in the experimental case. Furthermore, there is a large difference between the theoretical c_{33} values, and the c_{44}'s differ by about 5%, which is somewhat larger than in the experimental determinations. Although the results have not been included in Table XI, the same quality of agreement is found if the calculations are done in the self-consistent harmonic approximation or if the internal strain contributions are neglected. Also, it is expected that the inclusion of three-body forces would have the same effect in each case, thus having no consequence for the structural comparisons.[34] It is concluded therefore that the observed differences cannot be explained without considering the impurity molecules.

V. MODEL CALCULATIONS

This section comprises a description of the methods used, and the results obtained, in a theoretical investigation of some of the mechanisms that could account for the behavior of the experimentally determined c_{ij}'s. Since the treatment is of a preliminary nature, and was not intended to be exhaustive, only those effects most amenable to calculation have been considered. In particular, the consequences of relaxation of the host (Ar) lattice about the impurity molecules, and the effect of rotation-translation coupling have not been incorporated. It must also be pointed out that the approximations that are made preclude any high degree of (absolute) accuracy in the results for either phase; rather, it is the *differences* between calculated values for each structure, and the identification of the reasons for these differences, that will be emphasized.

A. Alloy model

The procedure adopted was to first develop a relatively simple model for pure Ar, and to then add impurity molecules. Guidance was provided, in part by the fact that the structural effects deduced from GK's calculations were similar in all levels of approximation, but mainly by the hope that at least some understanding of the important mechanisms present in this very complicated system could be identified within the simple model.

Each Ar atom was represented by a Lennard-Jones 6-12 potential.[89] The total potential energy of the crystal was calculated with interactions extending out to 4 (6) nearest-neighbor shells for the fcc (hcp) structure, so that each atom interacted with 54 (56) others out to a distance of twice the nearest-neighbor distance. The elastic constants were obtained by statically straining the matrix and taking appropriate derivatives. It was estimated that the total energy was converged to within about 2%; the convergence of the c_{ij}'s is indicated by error estimates in Table XII. An approximate analysis indicated that inclusion of the next neighboring shell in the hcp structure would not significantly improve these results. However, it is felt that this relatively poor convergence does not affect the conclusions drawn.

It was convenient to choose the unit cell to contain 56 sites, two of which were occupied by O_2 molecules, corresponding to an impurity concentration of about 5.6%, which is close to the experimental conditions. In the first of two configurations which were considered, the molecules were located so that the intermolecular distance was more than twice the nearest-neighbor distance, and therefore, no O_2-O_2 interaction was included. In the second configuration, they were located at the nearest-neighbor positions.

In contrast to the expected experimental conditions, these choices created an ordered structure in which, for example, $c_{11} \neq c_{22}$. Hence for each configuration, an average over the possible sites of the second molecule was taken, which was most easily done by taking the appropriately weighted averages of the c_{ij}'s for one such impurity.

The O_2 molecules were represented in a number of ways. The first and simplest was by a spherically symmetric Lennard-Jones potential[90] used to provide an indication of the effect of the differences in the average properties of O_2 and Ar, namely the well depth ϵ and range σ. For the O_2-Ar interaction these were taken, respectively, to be the geometric and arithmetic means of the corre-

TABLE XII. Elastic constants calculated using the model developed to investigate impurity effects (units: 10^9 N m^{-2}).

		Pure Ar	Spherical O_2	Sweet and Steele[a] 81.3 K	Jelinek *et al.*[b] 81.3 K	Cheung[b] 81.3 K	Laufer and Leroi[b] 2 K	81.3 K	10.000 K
fcc	$c_{11}(\pm 0.08)$	2.59	2.63	2.59	2.40	2.47	2.28	2.38	2.72
	$c_{12}(\pm 0.02)$	0.80	0.76	0.74	0.66	0.69	0.60	0.66	0.79
	$c_{13}(\pm 0.02)$	0.57	0.57	0.56	0.50	0.52	0.46	0.50	0.59
	$c_{33}(\pm 0.08)$	2.82	2.82	2.77	2.56	2.64	2.42	2.54	2.91
	$c_{44}(\pm 0.01)$	0.75	0.75	0.74	0.70	0.71	0.68	0.69	0.77
	c_{66}	0.90	0.94	0.92	0.87	0.89	0.84	0.86	0.96
hcp	$c_{11}(\pm 0.08)$	2.59	2.63	2.59	2.39	2.46	2.26	2.38	2.72
	$c_{12}(\pm 0.02)$	0.80	0.76	0.74	0.67	0.70	0.62	0.66	0.79
	$c_{13}(\pm 0.05)$	0.57	0.56	0.55	0.49	0.52	0.45	0.49	0.59
	$c_{33}(\pm 0.2)$	2.80	2.80	2.76	2.54	2.62	2.40	2.52	2.89
	$c_{44}(\pm 0.01)$	0.75	0.75	0.74	0.70	0.71	0.67	0.69	0.77
	c_{66}	0.90	0.94	0.92	0.86	0.98	0.82	0.86	0.96

[a]Reference 91.
[b]Referred to in Ref. 92.

sponding quantities for the O_2-O_2 and Ar-Ar interactions.

Atom-atom potentials were then used to incorporate the anisotropy of the molecules. For the O_2-O_2 interaction, these were of the usual form, whereas for the O_2-Ar potential,

$$V = 2\epsilon \sum_{i=1}^{2} \left[\left[\frac{\sigma}{r_i} \right]^{12} - \left[\frac{\sigma}{r_i} \right]^{6} \right] \tag{11}$$

was used, where the two distances r_i are those from each atom in the O_2 molecule to the Ar atom. The ϵ and σ were again taken as appropriate geometric and arithmetic means. Four different sets of parameters available in the literature were used, namely those proposed by Sweet and Steele, Laufer and Leroi, Jelinek *et al.*, and Cheung.[91,92]

The variation in energy with the orientation of the O_2 molecules was much less than the thermal energy (kT) at ~ 80 K, so the energy was thermally averaged over these orientations. By repeating the calculations at low T (2K), the experimental T (81.3 K) and very high T (10000 K), some information on the rotational smearing of the c_{ij}'s was obtained. It is emphasized that the host lattice was held frozen, so that no other temperature effects are included.

B. Results for the alloy model

The first test of this model was the calculation of the elastic constants for each structure of pure Ar, the results of which are presented in column 1 of Table XII. The important feature here is that, although the overall agreement with experiment, as expected, is not good, the results for the two structures *differ* at most, by less than 1%. Consequently, any further structural differences that are found within this model were presumed to be attributable to the impurities.

As a general result it was found that when oxygen was present there was never any significant difference in the elastic constants for the two different configurations. It is therefore concluded that there are no significant effects associated with the relative locations of the impurities which could account for the experimental results. Hence the results are presented only for one configuration, which was chosen to be the noninteracting one. This is not expected to be the case for N_2 impurities, as suggested in the next paragraph.

The results obtained when the impurity molecules were represented by the spherical Lennard-Jones potential are listed in the second column of Table XII. By comparison with pure Ar, it is apparent that the effects on the c_{ij}'s for each structure are small (0, 2, or 5%), and the differences between structures are insignificant. Although such impurity induced changes for each structure may be observable experimentally, there is no correlation with the results of Sec. III. In fact, even by combining these small differences with those found in the calculations of GK described earlier, the observed behavior cannot even approximately be reproduced. It is thus concluded that the size of the oxygen molecules does not have an important

effect. As an additional observation it can be noted that because of the small changes found when the molecule is included in this way, lattice relaxation is probably not a large effect. This contrasts with corresponding calculations that were performed for N_2 in Ar, in which the use of a Lennard-Jones potential for N_2 did cause significant changes in the elastic constants and energies, indicating larger contributions from lattice relaxation.

The results of calculations using the atom-atom potentials constitute the rest of Table XII. The c_{ij}'s corresponding to each of four different sets of potential parameters at 81.3 K are shown, and the effects of temperature for a representative potential, namely, that of Laufer and Leroi, are indicated in the last three columns. The latter effects were found to be qualitatively the same for each potential, so only one is discussed in detail. First of all, when the temperature was raised from 2 to 81.3 K, the elastic constants changed by up to 10%, and in the high-temperature limit by as much as 20% more. This clearly indicates important shape effects. However, there appear to be no significant structural effects. Among all the elastic constants, with four different sets of parameters at three different temperatures, the greatest difference between structures for any elastic constant is barely 2%, with no particular effect on either c_{13} or c_{33}.

From these calculations, in conjunction with the work of GK (Sec. IV), it may be concluded that there is evidence for a dependence of the c_{ij}'s on the structure of pure Ar, but the calculated effects do not adequately explain the behavior of the experimental c_{ij}'s for $Ar(O_2)$ mixtures. There consequently appear to be impurity effects beyond the stabilization of the hcp structure. However, no such effects were found within the model in which the O_2 molecules (either separated, or as nearest neighbors) undergo thermal rotation in a static, unrelaxed host. The remaining possibilities most likely to be important, are the static-lattice relaxation, which this work indicates is probably not very significant, and rotation-translation coupling. This represents more evidence of the importance of this mechanism, as has been discussed earlier.

VI. SUMMARY AND CONCLUSIONS

It has been determined that the single-crystal fcc phase of Ar accepts up to at least 4 mol % of O_2 (and N_2) and remains stable. Stable hcp single crystals could only be grown with not less than $\sim 5\%$ O_2 and N_2.[36]

The fcc elastic moduli are for the most part insensitive to changes in the concentration of O_2 (and N_2) up to about 4%. Mode softening is, however, reflected in the behavior of c_{44} with concentration, and this is especially the case with the addition of N_2, where phase instability was directly observed as a visible change from fcc-to-hcp.

The hcp elastic constants of $Ar_{0.94}(O_2)_{0.06}$ were determined to a high accuracy. It was found that, even at this high percentage of oxygen in the argon lattice, the elastic constants are consistent with pure argon values, except for c_{13} (and c_{13}/c_{44}). It is clear that any theoretical calculations should concentrate on this parameter. This was also evident from the β-CO and β-N_2 work.[64,65]

From model calculations presented here, it is shown that the change in structure either in the presence or absence of *spherical* O_2 impurity molecules, does not sufficiently affect the elastic constants to account for the experimental observations. When the elastic constants were calculated using *nonspherical* impurity interactions it was found that they did depend significantly on the thermal rotation of the impurities, thus showing that the anisotropy of the O_2 molecule plays a strong role in the intermolecular forces. A calculated *decrease* in c_{13}, however, was in contradiction to the experimental observation.

Anisotropic mechanisms that are clearly important and should be further considered are dynamical interactions of the host atoms with impurities in the form of rotation-translation coupling and, possibly relaxation of the host lattice about the impurity molecules. The latter effect is probably important for $Ar(N_2)$ but not for $Ar(O_2)$. The importance of the rotation-translation coupling effect is strongly supported by the low-frequency Raman spectra of $Ar(X_2)$ that show features associated with (1) the reorientation of impurity molecules and (2) impurity induced lattice vibrations of Ar (Ref. 67) and by the model calculations. Brillouin scattering studies of β-CO and β-N_2 (Refs. 64 and 65) and CH_4 and CD_4 (Ref. 71) and other theoretical calculations[68–70] are also consistent with the above.

It is, in general, expected that the anisotropic rotation-translation coupling has important implications for phase transitions and that c_{13}/c_{44} (for hexagonal symmetry, at least) is a sensitive measure of this effect. This appears to be the case for the fcc-hcp Ar system under study and most probably defines the role of diatomic impurity in stabilizing the hcp structure.

ACKNOWLEDGMENTS

The authors wish to express their gratitude to M. L. Klein for many stimulating discussions during the entire course of this work and for suggestions regarding theoretical calculations. Permission to refer to his unpublished results for pure Ar is greatly appreciated.

APPENDIX A: CALCULATION OF DENSITY

The concentration C_s of impurity in the crystal was estimated from the published phase diagrams,[56,57] and was also confirmed by observing the intensities of the Raman vibrational lines of O_2 and N_2 in the Ar matrix and comparing them with the intensity for the respective (pure) diatomic crystals.[62,63] The density of the alloy could then be calculated by a standard procedure[93] assuming substitutional impurities. The molecular weight of the alloy is given by

$$M_{AB}=C_sM_B+(1-C_s)M_A\ , \tag{A1}$$

where M_A is the molecular weight of the host atoms and M_B that of the impurity molecules. The volume of a unit cell V_c is a_0^3 for fcc and $a^2c\sin 60°$ for hcp crystals, a_0, a, and c being the lattice constants of the respective crystals. In addition, if it is assumed that in a transformation from fcc-to-hcp the density remains constant in Ar,[27] then for an ideal c/a ratio,

$$a=a_0/\sqrt{2}\ ,\quad c=1.633a\ . \tag{A2}$$

If Z is the number of atoms or molecules per unit cell, and A Avagadro's number, the density is given by

$$\rho=MZ/V_cA\ . \tag{A3}$$

For pure Ar, a_0 at various temperatures was calculated via an equation given in Ref. 27, from which the values of a and c were calculated using Eq. (A2). In order to calculate V_c, x-ray lattice constant measurements of $Ar(O_2)$ (Ref. 30) and $Ar(N_2)$ (Ref. 28) alloys were used. Since these constants were reported at low temperatures, the following procedure was used to calculate the density at higher temperatures. At a particular low temperature, the percentage difference in density between pure hcp Ar and doped hcp Ar was calculated. Assuming that this percentage difference would also exist at the scattering volume temperature T_s, a correction was made to the density of pure Ar at this temperature thus obtaining the density of the doped hcp crystal. A similar procedure was adopted for calculating the density of doped fcc Ar crystals.

It is to be noted that a difference between the measured bulk density of the solid and that calculated from the x-ray lattice constant measurements is to be expected mainly because of the concentration of vacancies. However, in pure Ar, it was found[94] that the two values differed by a very small amount, which was within the experimental errors. In fact, for pure Ar at 81.3 K, the bulk density measured by Smith and Chapman[95] was $1.6294\pm0.07\%\ \mathrm{g\,cm^{-3}}$, whereas the highly accurate x-ray lattice constant measurements of Peterson *et al.*[96] and similar measurements by Barrett and Meyer[27] give essentially the same value, i.e., $1.631\ \mathrm{g\,cm^{-3}}$. Since the Ar-alloy crystals were maintained within about 1.5 K of their freezing points, it was assumed that the effect of vacancy concentration on the density would be very small just as is the case in pure Ar.

APPENDIX B: CALCULATION OF REFRACTIVE INDEX

Refractive indices n for $Ar(O_2)$ and $Ar(N_2)$ solid solutions have not been experimentally investigated but values for pure Ar, O_2, and N_2 have been reported in the literature for various wavelengths and temperatures.[60,61] Therefore, the n values for the mixtures were calculated as follows.

For each component of the binary mixture, the first step was to choose three wavelengths (close to 5145.5 nm) at the desired temperature T (from a plot of n vs T). These were then used to calculate the three constants, r, s, and t in the Cauchy relation[97]

$$n=r+s/\lambda^2+t/\lambda^4\ . \tag{B1}$$

With the knowledge of these constants, the refractive index of the same component was calculated at $\lambda=514.5$ nm. Thus, for each pure component the refractive index at the desired wavelength was obtained.

The refractive index of the mixture was then obtained by the method of mixtures. For this the function F from the Lorentz-Lorenz relation[99]

$$\frac{M}{\rho}\frac{n^2-1}{n^2+2}=F \tag{B2}$$

(where F is the molar refractivity) was calculated for each component. If F^A and F^B corresponds to the components A and B, then the refractive index n_{AB} of the mixture[98,99] is given by

$$\frac{M_{AB}}{\rho_{AB}}\frac{n_{AB}^2-1}{n_{AB}^2+2}=C_S^B F^B+(1-C_s^B)F^A\ , \qquad \text{(B3)}$$

where C_s^B is the concentration of the B component.

Birefringence in doped hcp Ar crystals was studied by Hägele *et al.*[32] At 77 K and 2% O_2 in Ar, they reported

$$n_e-n_o=(2.11\pm0.63)\times10^{-6}\ ,$$

where n_e and n_o are extraordinary and ordinary refractive indices, respectively. In these experiments on hcp Ar alloy crystals, birefringence was found to be very small though detectable when the hcp crystal was viewed through crossed polaroids. The above value was considered negligible compared to the absolute value of n. No evidence of birefringence was observed in fcc Ar alloys.

[1] *Rare Gas Solids,* edited by M. L. Klein and J. A. Venables (Academic, London, 1976), Vols. I and II.

[2] K. F. Niebel and J. A. Venables, in *Rare Gas Solids,* Ref. 1, Vol. I, Chap. 9.

[3] T. Kihara and S. Koba, J. Phys. Soc. Jpn. 7, 348 (1952).

[4] L. Jansen and J. M. Dawson, J. Chem. Phys. 22, 1619 (1954).

[5] L. Jansen and J. M. Dawson, J. Chem. Phys. 23, 482 (1955).

[6] A. J. Prins, J. M. Dumore, and L. T. Tjoan, Physica (Utrecht) 18, 307 (1952).

[7] B. M. Axilrod, J. Chem. Phys. 19, 719 (1951); 19, 724 (1951).

[8] M. B. Doran and I. J. Zucker, J. Phys. C 4, 307 (1971).

[9] A. Hüller, Z. Phys. 241, 340 (1971).

[10] R. Howard, Phys. Lett. 29, A, 53 (1969).

[11] T. R. Koehler and R. L. Gray, Bull. Am. Phys. Soc. 16, 439 (1971).

[12] H. J. Schirlitzki, Z. Phys. 246, 363 (1971).

[13] V. V. Goldman, J. Phys. C 8, L119 (1975).

[14] T. H. K. Barron and C. Domb, Proc. R. Soc. London Ser. A 227, 447 (1955).

[15] C. Isenberg and C. Domb, J. Phys. Chem. Solids Suppl. 1, 141 (1965).

[16] C. Feldman, Proc. Phys. Soc. London 86, 865 (1965).

[17] L. Jansen, Phys. Lett. 4, 91 (1963); L. Jansen and S. Zimmering, *ibid.* 4, 95 (1963); L. Jansen, Phys. Rev. 135, A1292 (1964); L. Jansen and E. Lombardi, Chem. Phys. Lett. 1, 33 (1967).

[18] C. E. Swenberg, Phys. Lett. 24, A 163 (1967).

[19] J. Cuthbert and J. W. Linnett, Trans. Faraday Soc. 54, 617 (1958).

[20] T. Kihara, Adv. Chem. Phys. 5, 186 (1963).

[21] R. S. Knox and M. S. Reilly, Phys. Rev. 135, A166 (1964).

[22] K. F. Niebel and J. A. Venables, Proc. R. Soc. London Ser. A 336, 365 (1974).

[23] T. Bricheno and J. A. Venables, J. Phys. C 9, 4095 (1976).

[24] R. Mevrel, T. Bricheno, and J. A. Venables, J. Phys. C 10, 773 (1977).

[25] B. Borden and C. Radin, J. Chem. Phys. 75, 2012 (1981).

[26] L. Meyer, C. S. Barrett, and P. Haasen, J. Chem. Phys. 40, 2744 (1964).

[27] C. S. Barrett and L. Meyer, J. Chem. Phys. 41, 1078 (1964).

[28] C. S. Barrett and L. Meyer, J. Chem. Phys. 42, 107 (1965).

[29] C. S. Barrett and L. Meyer, J. Chem. Phys. 43, 3502 (1965).

[30] C. S. Barrett, L. Meyer, and J. Wasserman, J. Chem Phys. 44, 998 (1966).

[31] L. Meyer, Adv. Chem. Phys. 16, 343 (1969).

[32] W. Hägele, W. Probst, K. Dellian, J. Hingsammer, and E. Lüscher, Z. Naturforsch. 26a, 419 (1971).

[33] E. Schuberth, Phys. Status Solidi B 84, K91 (1977).

[34] V. V. Goldman and M. L. Klein, unpublished and private communication.

[35] R. A. Aziz and H. H. Chen, J. Chem. Phys. 67, 5719 (1977).

[36] S. F. Ahmad, H. Kiefte, and M. J. Clouter, J. Chem. Phys. 75, 5848 (1981).

[37] See, for example, M. Born and K. Huang, *Dynamical Theory of Crystal Lattices* (Clarendon, Oxford, 1954); I. L. Fabelinskii, *Molecular Scattering of Light,* translated by R. T. Beyer (Plenum, New York, 1968); H. Z. Cummins and P. E. Schoen, in *Laser Handbook,* edited by F. T. Arecchi and E. O. Schulz-dubois (North Holland, Amsterdam, 1972), Vol. II, p. 1030.

[38] G. B. Benedek and K. Fritsch, Phys. Rev. 149, 647 (1966).

[39] Chihiro Hamaguchi, J. Phys. Soc. Jpn. 35, 832 (1973).

[40] D. F. Nelson, P. D. Lazay, and M. Lax, Phys. Rev. B 6, 3109 (1972).

[41] L. D. Landau and E. M. Lifshitz, *Theory of Elasticity* (Pergamon, Oxford, 1970).

[42] A. G. Every, Phys. Rev. Lett. 42, 1065 (1979).

[43] J. F. Nye, *Physical Properties of Crystals* (Clarendon, Oxford, 1957).

[44] C. S. Barrett and T. B. Massalski, *Structure of Metals* (McGraw-Hill, New York, 1966).

[45] D. B. Novotny and J. F. Smith, Acta. Metall. 13, 881 (1965).

[46] H. J. Leamy and H. Warlimont, Phys. Status Solidi 37, 523 (1970).

[47] R. M. Martin, Phys. Rev. B 6, 4546 (1972).

[48] E. R. Fuller, Jr. and W. F. Weston, J. Appl. Phys. 45, 3772 (1974).

[49] R. W. G. Wyckoff, *Crystal Structures* (Interscience, New York, 1963) Vol. I.

[50]W. Tiller, in *The Art and Science of Growing Crystals,* edited by J. J. Gilman (Wiley, New York, 1963).
[51]H. Goldstein, *Classical Mechanics* (Addison-Welsey, Cambridge, 1950), p. 107.
[52]P. H. Gammon, Ph.D. thesis, Memorial University of Newfoundland, 1981 (unpublished).
[53]See, for example, J. R. Sandercock, in *Proceedings of the Second International Conference on Light Scattering in Solids, Paris, 1971,* edited by M. Balkanski (Flammarion, Paris, 1971); S. M. Lindsay and I. W. Shepherd, J. Phys. E 10, 150 (1977); C. Roychoudhri and M. Hercher, Appl. Opt. 16, 2514 (1977).
[54]W. May, H. Kiefte, M. J. Clouter, and G. I. Stegeman, Appl. Opt. 17, 1603 (1978).
[55]S. F. Ahmad, Ph.D. thesis, Memorial University of Newfoundland, 1980 (unpublished).
[56]F. Din, K. Goldman, and A. G. Monroe, Proceedings of the Ninth International Congress on Refrigeration, Paris, 1955, p. I-003.
[57]H. M. Long and F. S. Dipaolo, Chem. Eng. Prog. Symp. Ser. 59, 30 (1963).
[58]R. A. McLaren, Ph.D. thesis, University of Toronto, 1973 (unpublished).
[59]J. P. Franck and R. Wanner, Phys. Rev. Lett. 25, 345 (1970).
[60]A. C. Sinnock and B. L. Smith, Phys. Rev. 181, 1297 (1969); A. C. Sinnock, J. Phys. C 13, 2375 (1980).
[61]H. E. Johns and J. O. Wilhelm, Can. J. Res. 15, 101 (1937).
[62]H. Kiefte, M. J. Clouter, N. H. Rich, and S. F. Ahmad, Chem. Phys. Lett. 70, 425 (1980).
[63]H. Kiefte, M. J. Clouter, N. H. Rich and S. F. Ahmad, Can. J. Phys. (in press).
[64]H. Kiefte and M. J. Clouter, J. Chem. Phys. 64, 1816 (1976).
[65]P. H. Gammon, H. Kiefte, and M. J. Clouter, J. Chem. Phys. 70, 810 (1979).
[66]P. J. Thomas, S. C. Rand, and B. P. Stoicheff, Can. J. Phys. 56, 1494 (1978).
[67]N. H. Rich, M. J. Clouter, H. Kiefte, and S. F. Ahmad. Bull. Am. Phys. Soc. 27, 633 (1982); Can. J. Phys. (in press).
[68]M. L. Klein and J. J. Weis, J. Chem. Phys. 67, 217 (1977).
[69]V. V. Goldman and M. L. Klein, J. Chem. Phys., 64, 5121 (1976).
[70]O. Schnepp and A. Ron, Discuss. Faraday Soc. 48, 26 (1969).
[71]S. C. Rand and B. P. Stoicheff, Can. J. Phys. 60, 287 (1982).
[72]S. Gewurtz and B. P. Stoicheff, Phys. Rev. B 10, 3487 (1974).
[73]H. R. Moeller and C. F. Squire, Phys. Rev. 151, 689 (1966).
[74]G. H. Keeler and D. N. Batchelder, J. Phys. C 3, 510 (1970).
[75]Y. Fujii, N. A. Lurie, R. Pynn and G. Shirane, Phys. Rev. B 10, 3647 (1974).
[76]H. Meixner, P. Leiderer, P. Berkerich, and E. Lüscher, Phys. Lett. 37A, 39 (1971); 40, 257 (1972).
[77]R. A. Fisher and R. O. Watts, Mol. Phys. 23, 1051 (1972).
[78]Y. Yamada, M. Mori, and Y. Noda, J. Phys. Soc. Jpn. 32, 1565 (1972).
[79]M. L. Klein and R. D. Murphy, Phys. Rev. B 6, 2433 (1972).
[80]T. G. Gibbons, M. L. Klein, and R. D. Murphy, Chem. Phys. Lett. 18, 325 (1973).
[81]J. A. Barker and A. Pompe, Aust. J. Chem. 21, 1683 (1968).
[82]J. A. Barker, R. A. Fisher, and R. O. Watts, Mol. Phys. 21, 657 (1971).
[83]J. M. Parson, P. E. Siska, and Y. T. Lee, J. Chem. Phys. 56, 1511 (1972).
[84]M. L. Klein and T. R. Koehler, in *Rare Gas Solids,* Ref. 1, Vol. I, Chap. 6.
[85]V. V. Goldman, J. Low Temp. Phys. 26, 203 (1977).
[86]H. R. Glyde and V. V. Goldman, J. Low Temp. Phys. 25, 601 (1976).
[87]M. L. Klein, G. K. Horton, and V. V. Goldman, Phys. Rev. B 2, 4995 (1970).
[88]G. Liebfried and W. Ludwig, in *Solid State Physics,* edited by F. Seitz and D. Turnbull (Academic, New York, 1961), Vol. 12, p. 313.
[89]J. A. Barker, in *Rare Gas Solids,* Ref. 1, Vol. I, Chap. 4.
[90]J. O. Hirschfelder, C. F. Curtiss, and R. B. Bird, *Molecular Theory of Gases and Solids* (Wiley, New York, 1954).
[91]J. R. Sweet and W. A. Steeles, J. Chem. Phys. 47, 3022 (1967).
[92]K. Kobashi and M. L. Klein, J. Chem. Phys. 71, 843 (1979).
[93]F. D. Bloss, *Crystallography and Crystal Chemistry* (Holt, Rinehart and Winston, New York, 1971).
[94]A. V. Chadwick and H. R. Clyde, in *Rare Gas Solids,* Ref. 1, Vol. II, Chap. 19.
[95]B. L. Smith and J. H. Chapman, Philos. Mag. 15, 739 (1967).
[96]O. G. Peterson, D. N. Batchelder, and R. O. Simmons, Phys. Rev. 150, 703 (1966).
[97]R. W. Ditchbrun, *Light* (Academic, London, 1976), p. 47.
[98]L. E. Nielsen, *Predicting the Properties of Mixtures: Mixture Rules in Science and Engineering* (Dekker, New York, 1978).
[99]M. Born and E. Wolf, *Principles of Optics* (Macmillan, New York, 1964), p. 87.